Studies on the Activation of Mn-Promoted Sulfated Zirconia Catalyst for Alkane Isomerization by *In-Situ* UV-vis-NIR Spectroscopy

Masterarbeit

Am Fachbereich Biologie, Chemie, Pharmazie der Freien Universität, Berlin
zur Erlangung des akademischen Grades
Master of Science

Vorgelegt von

Joshi Pradnya

February, 2005

Betreuer: Prof. Dr. J. Simon
Prof. Dr. P. Roesky

This work was carried out at Department of Inorganic Chemistry, Fritz-Haber-Institut der Max-Planck-Gesellschaft, Berlin, Germany, from 10th May 2004 to 10th February 2005 under the kind supervision of **Dr. A. Trunschke.** This thesis would not have been possible without the help of many people. I sincerely acknowledge them.

First, I would like to express my deep gratitude to my guide and supervisor, **Prof. Dr. J. Simon.** His encouragement and guidance were the driving forces of my success. Under his shelter, I enjoyed my learning at Department of Inorganic Chemistry, Freie Universität, Berlin. My sincere thanks to **Prof. Dr. P. Roesky** who agreed to be a member of my supervisory committee. I am indebted to **Prof. Dr. R. Schlögl and Dr. F. Jentoft** who gave me an excellent opportunity to work at the Fritz-Haber-Institut. In the everyday work at the Fritz-Haber-Institut I benefited enormously from the discussions with **Dr. A. Trunschke** and with **Dr. F. Jentoft** and in fact because of their kind guidance and support made the completion of this thesis. I am grateful to **Prof. Dr. Sophia Klokishner** who worked hard for the band assignments of UV-vis-NIR spectra obtained during measurements.

I also express my gratitude to my colleagues from the Fritz-Haber-Institut **G. Lorenz, Dr. R. Jentoft, Dr. R. Horn, Dr. S. Wrabetz, Dr. G. Tzolova-Müller, R. Lloyd, B. Klose, J. Kröhnert, C. Chan Thaw, O. Kirilenko, E. Rödel, J. Osswald, Dr. V. Makwana and Dr. S. Vijay** and working with them was a pleasant experience. I would like to thank **Katrin**, **Sameer**, **Rhys** and **Peter** for their many favors; especially in the days of thesis writing. I thank **Dila and Nurain** for their friendship and we spent together many happy days.

I remember the warmth and help of **Prof. Dr. K. Christmann**, **Prof. Dr. Hans-Heinrich Limbach**, **Ms. Caroline Friedrich, Dr. Boaz Paz, Suhana Reddy and Claudia Swart,** from the Institut für Chemie, Freie Universität, Berlin, during scientific and non-scientific encounters.

I can not complete this session without including my school teacher, **Mr. S. N. Atre, Dr. R. V. Chaudhari, Dr. C. V. Rode and Dr. V. H. Rane** from National Chemical Laboratory, Pune, India. I really have no words to thank you all for your constant support and encouragement. Thank you so much for being there always for me.

I take this opportunity to thank my friends, *Manisha, Shrikant, Anvita, Rohit, Yogita, Prashant, Deepti and Sanjeev* for their love and encouragement.

This list would by no means be complete without thanking to all my family members and my warmest thanks to my in laws and to my sister, twin brothers for their love and support.

Last but not least I have to thank three people without them this is an impossible task: my husband, *Mangesh and my parents.* I am dedicating this small but very important work in my life to them.

CONTENTS

Abstract

In this thesis, Mn-promoted sulfated zirconia (0.5 wt% Mn) was investigated during activation in inert (He) and oxidizing atmosphere (O_2) at 773 K and during subsequent *n*-butane isomerization (323 K, 1 kPa *n*-butane) using *in-situ* UV-vis-NIR diffuse reflectance spectroscopy. At first, a few experiments were carried out to test the newly installed Harrick Praying Mantis Set-up for *in-situ* UV-vis-NIR investigations of *n*-butane isomerization over the catalyst.

In its initial state, i.e. after calcination and exposure to ambient conditions, the catalyst contains mainly Mn^{3+} and presumably small amounts of Mn^{2+} as well as adsorbed water. Activation in O_2 only dehydrates the catalyst, while activation in He additionally leads to partial reduction of manganese (formation of new species Mn^{2+}). Mn-SZ activated in pure O_2 exhibits a maximum isomerization rate of 220 µmol $g^{-1}h^{-1}$; activation in He only yields a maximum rate of 100 µmol $g^{-1}h^{-1}$. With time on stream, the catalyst first passes through a phase of rapidly increasing conversion (induction period), then through a conversion maximum followed by partial deactivation to a steady state. Induction period was found to depend on the activation atmosphere and the *n*-butane concentration in the feed. During the period of maximum activity, propane and pentanes were observed as by-products. During the periods of low activity in the beginning and at long time on stream, the high selectivity to isobutane was observed.

Chapter 1

Introduction

1.1 Isomerization of *n*-alkanes

Isomerization of straight chain alkanes to their branched isomers is of great industrial importance because the branched alkanes are used themselves as fuel components, or in the manufacture of gasoline additives. For instance, isobutane formed by isomerization of *n*-butane is a key component for the manufacture of valuable gasoline additives such as trimethylpentanes and methyl *tert*-butyl ether (MTBE). The catalysts used in the commercial processes that produce branched hydrocarbons still suffer from several disadvantages particularly related to environmental problems. For example, a commercial catalyst for the isomerization of lower *n*-alkanes is Pt/chlorinated-Al_2O_3, which is sensitive to water and requires constant addition of toxic and corrosive alkyl chlorides to recover acid functionalities [1]. Alkane isomerizations are also catalyzed by liquid superacids, which are prepared by combining already strong fluorinated Brönsted acids such as HF, HSO_3F, CF_3SO_3H with strong Lewis acids such as SbF_5, TaF_5, AsF_5. However, these superacids are undesirable as industrial catalysts due to corrosion, handling, separation and disposal problems.

Therefore, strongly acidic solid catalysts have been developed to avoid the disadvantages of the mineral acids. The solid acids are not aggressive as the liquid acids, even though being stronger, since the acid sites are hidden inside the well-developed catalyst pore structure [2]. Their repeated use is possible and their separation from liquid products is much easier. Furthermore, they can be designed to give higher activity, selectivity, and longer catalyst life. Since the past 20 years, many classes of solid acid catalysts like acid-treated clays, zeolites, ion-exchange resins and metal oxides have been developed, characterized and applied for various hydrocarbon reactions [3]. Amongst these, sulfated zirconia (denoted as SZ hereafter) and modified SZ form an important class of catalysts and the importance of these catalysts for environmentally benign processes is highlighted in a number of reviews [4, 5, 6].

1.2 Sulfated Zirconia Catalysts

Zirconium oxide, ZrO_2, is a very interesting material because of its thermal stability, mechanical properties, and its basic, acidic, reducing and oxidizing surface properties [7]. The acid-base bifunctional nature of the ZrO_2 surface can be very useful for acid-base-catalyzed reactions and has been discussed in detail by Tanabe and Yamaguchi [8]. Anions such as SO_4^{2-} can be adsorbed on the ZrO_2 surface and the most commonly used sulfating agents are H_2SO_4 and $(NH_4)_2SO_4$. The addition of the sulfate ion, SO_4^{2-} to zirconia produces a very strong acid, which can catalyze reactions demanding high acidity, such as alkane isomerization [9].

Besides, generating strong acidity, SO_4^{2-} ions also stabilize the tetragonal phase of zirconia [5]. Zirconia exhibits three different crystalline polymorphs: monoclinic (*m*), stable at temperatures below 1373 K; tetragonal (*t*) stable at temperatures between 1373 and 2173 K; and cubic (*c*), stable above 2173 K. Nevertheless, the *t* and *c* forms can be generated and maintained as metastable structures at much lower temperatures than those mentioned above [7]. In the usual preparation of ZrO_2 catalysts through calcination of an amorphous hydroxide precursor at 723-923 K, the tetragonal phase or a mixture of *m* and *t* phases is obtained. Initially it was believed that only the tetragonal phase is catalytically active in sulfated zirconia but later *m*-ZrO_2 was also shown to be equally active [10].

By using Hammett acidity functions (*Ho*), Arata and co-workers [9] reported that SZ is a *superacid* and shows an acid strength (*Ho* = -16) higher than the acid strength of 100% sulfuric acid. They claimed that due to this strong acidity, SZ is capable of catalyzing the isomerization of n-butane to isobutane at room temperature. This catalytic performance is unique compared to typical solid acid catalysts, such as zeolites, which show no activity for the reaction at such low temperatures [5]. The low-temperature activity is very favorable since the equilibrium shifts to branched isomers at lower temperature [13]. Since the discovery of its strong acidity, SZ has attracted much attention as a potential process catalyst. It is found to be well suited for catalyzing many industrially important reactions, e.g. hydrocarbon isomerization, methanol conversion to hydrocarbons, alkylation, acylation, esterification, etherification, condensation, nitration and cyclization [6].

1.3 Promoted Sulfated Zirconia

Promoters are materials that enhance the activity of the catalyst, usually with a simultaneous increase in selectivity. Their role is complex and they constitute only a small part of the whole catalyst (typically 5 to 25 per cent by weight of the whole) but have a profound impact on the overall reactivity or selectivity of the catalyst. They can be divided into structural promoters and chemical promoters. Chemical promoters may have been added to the catalyst to optimize its activity and selectivity, and structural promoters may have been incorporated to improve the mechanical properties and stabilize the particles against sintering [11,12].

Addition of some promoters to SZ may result in a greatly improved catalytic performance and a number of studies mentioned that iron and manganese are the most effective promoters. Hsu et al. [14] claimed that the SZ containing Mn and Fe is about three orders of magnitude more active than SZ at 301 K. They claimed the higher acidity from the result of TPD of benzene. Lange et al. [15] reported that the activity of SZ for *n*-butane isomerization can be further enhanced by addition of first-row transition metal cations such as Mn, Fe, Co, Ni and Zn. They found that iron and manganese are the two most active promoters as compared to other and the promoting effect decreased from left to right in the periodic table. All promoted catalysts are similarly selective and predominantly produce isobutane, with propane and pentanes as side products.

Extensive research has been carried out to elucidate the origin of the high activity of Mn and Fe promoted SZ. Initially, an increase in acidity due to these promoters was thought to be the main reason for increased activity of the catalyst [16, 17]. Later Wan et al. [18] proposed the introduction of a redox function as the reason behind the increased catalytic activity for alkane isomerization. According to this hypothesis, traces of butenes are formed in an oxidative dehydrogenation of *n*-butane, which are converted into carbenium ions, which act as chain carriers for the isomerization of *n*-butane (shown in Scheme 1).

Many studies point toward an interplay of redox and acidic sites of promoters but no clear picture has evolved, and the action of the promoter is still unknown.

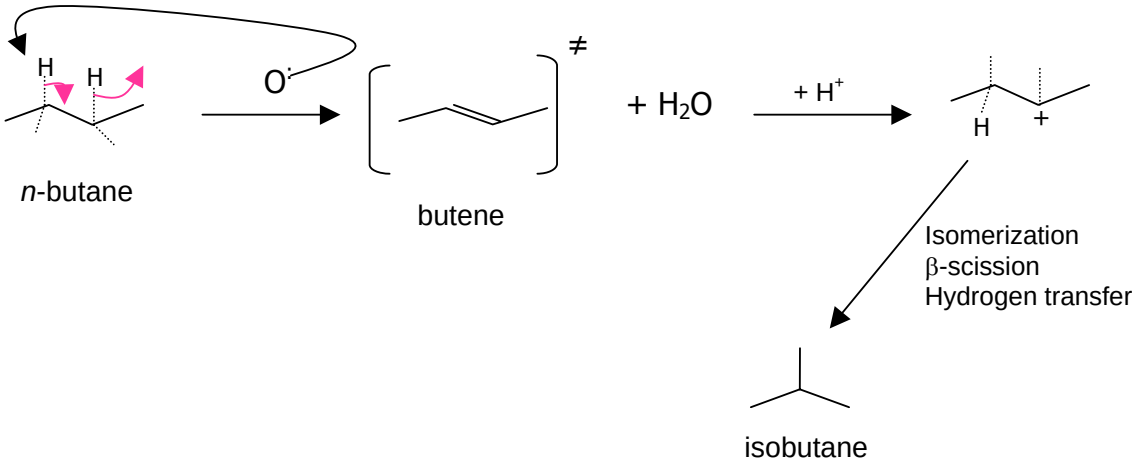

Scheme 1 Oxidative dehydrogenation of *n*-butane

1.4 Deactivation

The classic definition of a catalyst is a substance that alters the rate at which a chemical reaction occurs, but itself remains unchanged at the end of reaction. It is a practical reality, however, that catalysts deactivate over time. Sulfated zirconia and promoted sulfated zirconia catalysts are active for the conversion of *n*-butane into isobutane at low temperature, but unfortunately, suffer from rapid deactivation (within 30-120 min on stream). Several suggestions have been made in order to explain the deactivation process, among them: (i) formation of hydrocarbon surface deposits (coke) (ii) reduction of $Zr^{4+} \longrightarrow Zr^{3+}$ at the surface by the reacting hydrocarbon (iii) reduction of the surface sulfate groups and H_2S formation (iv) change in the surface phase of zirconia from tetragonal to monoclinic and (v) surface poisoning by water [19]. A number of studies indicate that the deactivation is mostly caused by coke formation during isomerization [20,21]. It is now widely accepted that *n*-butane isomerization occurs via a bi-molecular pathway, in which *n*-butane undergoes dehydrogenation to form unsaturated intermediates. These intermediates subsequently lead to the formation of coke. Deactivation of promoted catalysts can also be envisioned by reduction of the promoter in a stoichiometric redox reaction, which initiates the catalytic cycle.

1.5 Goals and work strategy

In spite of numerous research papers and reports available since the early 90s on the *n*-butane isomerization via iron-and/or manganese-promoted sulfated zirconia, there is still no clear understanding of some aspects, such as the role of promoters, proper description of reaction mechanism and the main cause of catalyst deactivation. According to a hypothesis by Wan et al [18], if *n*-butane isomerization proceeds via oxidative dehydrogenation (ODH), water and butene would have to be formed (shown in Scheme 1) and a catalyst component such as the promoter, zirconium or sulfate would have to be reduced. The present study is a ***primary step taken to check for indications of ODH***, i.e. reduction of manganese and formation of water. The work is focused on the following aspects:

1) Installation and test of a new set-up for *In-situ* UV-vis-NIR *Diffuse Reflectance* Spectroscopy.
2) Monitoring the catalyst especially the changes of the manganese oxidation state during activation.
3) Evaluating the influence of different pretreatment atmospheres on the performance of the catalyst.
4) Understanding of the simple aspects of deactivation by monitoring the manganese oxidation state, formation of water and unsaturated species during *n*-butane isomerization.

We selected a system promoted with manganese (0.5 wt % Mn) and used ***In-situ UV-vis-NIR Diffuse Reflectance Spectroscopy*** to monitor the catalyst and the formation of water. For evaluation of the role of the manganese oxidation state, oxidizing as well as inert conditions were employed in the activation procedure. Isomerization of *n*-butane at 323 K was used as a test reaction and analysis of the gas phase products was performed by on-line gas chromatography.

1.6 Organization of thesis

The thesis is structured as follows:

1) Theoretical background and experimental set up of *in-situ* UV-vis-NIR diffuse reflectance spectroscopy are explained in **Chapter 2.**
2) Catalyst preparation, methods used for the characterization and the results obtained are described in **Chapter 3.**
3) Results and discussion from the activation of Mn-SZ catalyst and *n*-butane isomerization by *in-situ* UV-vis-NIR diffuse reflectance spectroscopy are shown in **Chapter 4.**
5) Summary and Outlook are given in **Chapter 5**.

The following abbreviations will be used in the thesis:

Name	Abbreviation
Zirconia	ZrO_2
Sulfated Zirconia	SZ
Manganese-promoted Sulfated Zirconia	Mn-SZ
near-IR	NIR

References

1. M. Hino, K. Arata, Green Chemistry, 3 (2001) 170.
2. Sameer Vijay, Ph.D Dissertation, University of Notre Dame,Indiana, 2004.
3. K. Tanabe, W. F. Hölderich, Appl. Catal. A: General, 181 (1999) 399.
4. A. Corma, Chem. Rev., 95 (1995) 559.
5. X. Song, A. Sayari, Cata. Rev.-Sci. Eng., 38(3) (1996) 329.
6. G. D. Yadav, J. J. Nair, Microporous and Mesoporous Materials, 33 (1999) 1.
7. R. A. Comelli, C. R. Vera, J. M. Parera, J. Catal., 151 (1995) 96.
8. K. Tanabe, T. Yamaguchi, Catal. Today, 20 (1994) 185.
9. M. Hino, K. Arata, J. Am. Chem. Soc., 101 (1979) 6439.
10. B. S. Klose, R. E. Jentoft, A. Hahn, T. Ressler, J. Kröhnert, S. Wrabetz, X. Yang, and F. C. Jentoft, J. Catal., 217 (2003) 487.
11. G. C. Bond, Heterogeneous Catalysis: principles and applications, Oxford University Press, (1974) 103.
12. I. Chorkendorff, J. W. Niemantsverdriet (Eds.), Concepts of Modern Catalysis and Kinetics, Wiley-VCH, (2003) 129.
13. Y. Ono, Cata. Today, 81 (2003) 17.
14. C.-Y. Hsu, R. Heimbuch, G.T. Gates, J. Chem. Soc., Chem. Commun. (1992) 1645.
15. F. C. Lange, T. -K. Cheung, B.C. Gates, Catal. Lett., 41 (1996) 95.
16. T. -K. Cheung, J. L. d'Itri, B. C. Gates, J. Catal., 151 (1995) 464.
17. F. C. Jentoft, A. Hahn, J. Kröhnert, G. Lorenz, R. E. Jentoft, T. Ressler, U. Wild, R. Schlögl, C. Häßner and K. Köhler, J. Catal., 224 (2004) 124.
18. K. T. Wan, C. B. Khouw and M. E. Davis, J. Catal., 158 (1996) 311.
19. R. Ahmad, J. Melsheimer, F. C. Jentoft and R. Schlögl, J. Catal., 218 (2003) 365.
20. K. B. Fogash, Z. Hong, J. M. Kobe, J. A. Dumesic, Appl. Catal. A: General, 172 (1998) 107.
21. S. Y. Kim, J. G. Goodwin Jr., D. Galloway, Catal. Today, 63 (2000) 21.

Chapter 2

In-Situ UV-vis-near-IR Diffuse Reflectance Spectroscopy

2.1 Introduction

Understanding how activity and selectivity in catalytic reactions depend on structural and electronic properties of the catalyst is one of the major goals in catalysis research. This can be achieved by studying catalytic materials, while the catalytic reaction is running i.e. by ***In-Situ Spectroscopy***. With the help of *in-situ* techniques, one can monitor the various events taking place in catalytic materials such as changes in oxidation state of the working catalyst and observation of adsorbed reaction intermediates or side products under reaction conditions [1]. The molecular structure of a catalyst is very dynamic and readily transforms if the surrounding environment is changed. The presence of water, oxygen or other molecules may completely alter the molecular structure of a catalyst. Therefore, measuring a catalyst outside the reactor (***ex-situ analysis***) is mostly of little relevance to yield a reliable picture of the catalytic system under reaction conditions. The field of *in-situ* spectroscopy is under strong development and of high interest to the catalysis community.

In the present work, we have employed *in-situ* UV-vis-near-IR diffuse reflectance spectroscopy (*in-situ* DRS) to study the Mn-SZ catalyst. This is a suitable technique for studying electronic transitions (d-d, charge transfer transitions) of manganese ions [2, 3]. Additionally, it is a useful method for the detection of hydrocarbon surface deposits (coke) and adsorbed water during *n*-butane isomerization [4]. The acquisition of UV-vis-near-IR diffuse reflectance spectra in *in-situ* form (measurement can be taken at any temperature and atmosphere and on line GC analysis), could be the key in understanding the isomerization reaction pathway and the active nature of the catalyst.

2.2 Theory

2.2.1 Theoretical Background of Ultraviolet -Visible (UV-vis) Spectroscopy

As shown in Fig. 2.1, the absorption of electromagnetic radiation of wavelengths 200-800 nm (U. V. and visible region) can cause excitation of valence electrons from a low energy **H**ighest **O**ccupied **M**olecular **O**rbital (HOMO) to a high energy **L**owest **U**noccupied **M**olecular **O**rbital (LUMO).

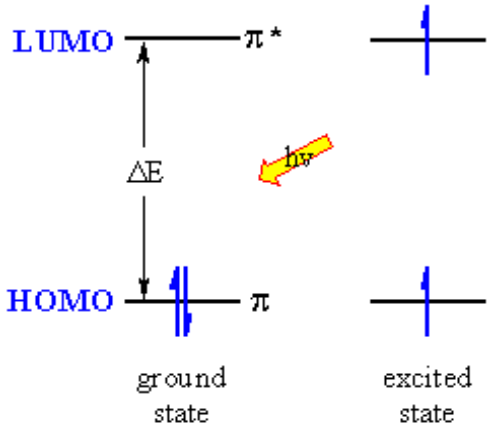

Figure 2.1 Electronic excitation

There are three kinds of electrons present in molecules,

i) σ electrons – present in σ-bonds.

ii) π electrons – present in π-bonds.

iii) '*n*' non-bonding electrons – present as unshared electrons.

Sigma (σ) and pi (π) electrons have corresponding higher energy antibonding molecular orbitals (σ*, π*) but there is no higher energy antibonding molecular orbital corresponding to non-bonding electrons. The total energy required for excitation of a molecule from ground state to excited state is given by *Born-Oppenheimer approximation*:

$$E = E_{electronic} + E_{vibrational} + E_{rotational}$$

Each electronic level of excitation consists of a number of vibrational levels and each vibrational level consists of a number of rotational levels. Absorption of ultraviolet and visible radiation in organic molecules is restricted to certain functional groups (*chromophores*) that contain valence electrons of low excitation energy. The spectrum of a molecule containing these chromophores is complex.

This is because the superposition of rotational and vibrational transitions on the electronic transitions gives a combination of overlapping lines. This appears as a continuous absorption band. Possible electronic transitions of π, σ, and *n* electrons are shown in Fig. 2.2.

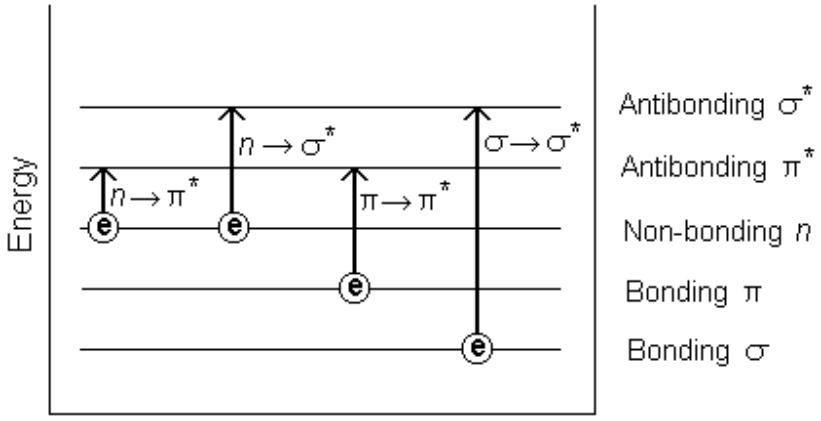

Figure 2.2 Possible electronic transitions of π, σ, and *n* electrons

From the above different types of transitions, only $n \rightarrow \pi^*$ *and* $\pi \rightarrow \pi^*$ *transitions* are concerned with the present work and hence discussed in detail. The other three types of transitions that are discussed are:

- Transitions involving charge-transfer electrons
- Transitions involving d and f electrons
- Vibrational transitions in the near-IR range

n* → π* *and* π → π* *Transitions

Most absorption spectroscopy of organic compounds is based on transitions of *n* or π electrons to the π^* excited state. This is because the absorption bands for these transitions fall in an experimentally convenient region of the spectrum (200 - 700 nm).

These transitions need an unsaturated functional group in the molecule to provide the π orbitals. Compounds containing double bonds involving hetero atoms such as O, N, S, halogen etc. undergo $n \rightarrow \pi^*$ transitions. Compounds having multiple bonds undergo $\pi \rightarrow \pi^*$ transitions e.g. alkenes, alkynes, carbonyl compounds, nitriles and aromatic compounds. Also organic and inorganic ligands attached to metals show intense $n \rightarrow \pi^*$ and $\pi \rightarrow \pi^*$ transitions in the UV region [5].

Transitions involving charge-transfer electrons

Many inorganic complexes show charge-transfer absorption and are called charge-transfer complexes. For a complex to demonstrate charge-transfer behavior one of its components must have electron donating properties and another component must be able to accept electrons. Absorption of radiation then involves the transfer of an electron from the donor to an orbital associated with the acceptor. As a consequence, the excited state is the product of a kind of internal oxidation/reduction process. Three types of charge-transfer are known; i) Ligand to metal charge transfer (LMCT) ii) Metal to Ligand charge transfer (MLCT) and iii) Metal to metal charge transfer (MMCT). MMCT transitions are sometimes called intervalence transitions, e.g. Fe^{2+} to Fe^{3+} in Fe_3O_4 or Fe^{2+} to Ti^{4+} in sapphire. The first two types can be detected in the range 200-400 nm and the last one in the range 400-800 nm. Common examples of such complexes include the thiocyanate and phenolic complexes of iron (III) or the iodide complex of molecular iodine.

Transitions involving d and f electrons

Most transition – metal ions absorb in the ultraviolet or visible region. For the lanthanide and actinide series, the absorption is caused due to the electronic transitions of 4*f* and 5*f* electrons; for the first and second transition metal series, the 3*d* and 4*d* electrons are responsible. Transitions between 3d-states are of great influence on the optical properties and often determine the color of the compounds.

The energy required to promote electrons from one *d* level to another *d* level of higher energy is very low and so light is absorbed in the visible region. The color of a transition metal complex is dependent on the energy difference between the two *d* levels.

This in turn depends on the nature of the ligand and on the type of complex formed. Some transition metal compounds are white, e.g. $ZnSO_4$ and TiO_2 due to absence of *d* - *d* transitions. The zinc ion has a d^{10} configuration and full *d* levels. On the other hand Ti^{4+} has a d^{0} configuration and empty *d* levels. Furthermore, *d* - *d* transitions give information on oxidation states and symmetry of the transition metal ion.

Vibrational transitions in the near-IR range

NIR is the wavelength region between 800-2500 nm in which absorptions corresponding to overtones and combinations of stretching and bending vibrations can be observed. In NIR-diffuse reflectance spectroscopy, surface groups such as OH, SH, NH are easily detected as well as the overtones and combinations of vibrations of ligands employed in catalyst preparation [5].

2.2.2 Phenomenon of Diffuse Reflectance

Diffuse reflectance spectroscopy is an effective way of obtaining infrared and UV-VIS spectra directly on powdered samples with a minimum of sample preparation. It is particularly effective for powders with a high surface area. This makes diffuse reflectance a valuable tool for catalysis, oxidation, and photochemical studies. Reflection of radiation is of four types: *specular reflection, diffuse reflection, internal reflection and attenuated total reflection* [6.7].

Diffuse reflection is a complex process that occurs when a beam of radiation strikes the surface of a finely divided powder. The radiation reflected from a powdered surface consists of two components: the specular component that is reflected from the surface and the diffuse component that is absorbed into the material and reappears at the surface after multiple scattering. Reflection off of smooth surfaces such as mirrors or a calm body of water leads to a type of reflection known as *specular reflection*. Reflection off of rough surfaces such as clothing, paper, and the asphalt roadway leads to a type of reflection known as *diffuse reflection* (Fig.2.3).

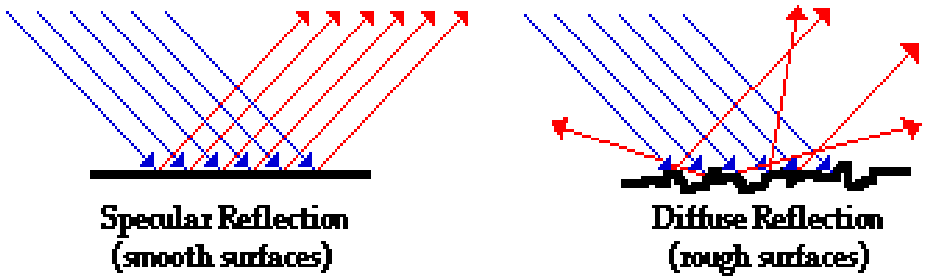

Figure 2.3 Specular and diffuse reflection

The specularly reflected component is just directionally scrambled reflectance (i.e. diffused) and hence is described by the Fresnel equations. Experimental methods that avoid or at least suppress the influence of the specular component collect the true diffuse reflectance spectra.

Those that collect a combination of the diffuse and specular components are often also referred to as 'diffuse reflectance,' but are perhaps more correctly named in-line diffuse reflectance. The diffusely reflected component is theoretically described by the widely used **Kubelka-Munk theory** [8]. The Kubelka-Munk equation is expressed as follows:

$$F(R_\infty) = \frac{(1-R_\infty)^2}{2R_\infty} = \frac{K}{S}$$

Where,

R_∞ = diffuse reflectance of the sample layer relative to a nonabsorbing standard

K = molar absorption coefficient of the sample

S = scattering coefficient

The Kubelka-Munk equation creates a linear relationship for spectral intensity relative to sample concentration by assuming infinite sample dilution in a non-absorbing matrix, a constant scattering coefficient and an “infinitely thick” sample layer. These conditions can be achieved for highly diluted, small particle samples (the scattering coefficient is a function of sample size and packing) and a sample layer of few millimetres of thickness. With proper sample preparation diffuse reflectance spectroscopy can provide ppm sensitivity and high quality results.

2.2.3 Gas Chromatography

Chromatographic techniques are widely used for the separation and identification of chemical compounds due to many advantages over other methods such as speed, simplicity and relatively low cost. In gas chromatography, the compounds to be analyzed are vaporized and eluted through the column by the flow of an inert, gaseous mobile phase. The column itself contains a liquid stationary phase that is adsorbed onto the surface of an inert solid. As the analytes are swept through the column by the mobile phase, separation occurs based on the affinity of each analyte for the stationary phase. As individual components of the mixture elute the chromatographic column, they are carried to a detector. The detector generates a measurable electrical signal, referred to as peaks, that is proportional to the amount of analyte present. Detector response is plotted as a function of the time required for the analyte to elute from the column after injection. The resulting plot is called a chromatogram. The position of the peaks on the time axis may serve to identify the components and the area under the peaks provide a quantitative measure of the amount of each component.

In the present study we used a flame ionization detector, which is the most widely used and generally applicable detector for gas chromatography. It is a useful detector for the analysis of organic compounds; it has high sensitivity, a large linear response range, and low noise. It is also robust and easy to use and the only drawback is, it destroys the sample. The detection principle is based on the production of ions in a flame and the current resulting from the pyrolysis of any organic compounds is measured.

The column used was Porous Layer Open Tubular (PLOT) capillary column. These columns are fused silica capillary columns ideal for separation of alcohols, free fatty acids, halogenated compounds, hydrocarbons C_1-C_6, ketones and sulfur compounds. They have the advantages of physical strength, low reactivity and flexibility (can be wound into coils).

2.3 Experimental

2.3.1 Measurement Details

In-situ UV-vis-NIR diffuse reflectance spectra were acquired with a PerkinElmer Lambda 9 spectrometer equipped with a Harrick Praying Mantis™ **diffuse reflectance attachment** type DRA-4-PE7 and HVC-DR3 **reaction chamber**. The diffuse reflectance attachment along with the reaction chamber is described in section **2.3.2**. All spectroscopic measurements were carried out sequentially over the range of 250 - 2500 nm with a scan speed of 240 nm min^{-1}, a nominal slit width of 2.0 nm (in the range 200-800 nm), and a step width of 2 nm (in the range 800-2500). A photomultiplier tube serves as a detector in the UV-vis range, while a PbS detector was employed in the NIR range. The detector and grating switch was set to 860 nm.

The reflectance technique requires the use of a white standard to which the sample is compared, ideally a material that reflects the light diffusely over the desired wavelength range. In this work, we used Spectralon® (Labsphere) as a reflectance standard for base line correction. It is a chemically inert thermoplastic resin and has typical reflectance values of 95% to 99% with relatively flat spectral distribution over the UV-vis-NIR region of the spectrum. In addition, its extremely hydrophobic nature leads to exclusion of water overtone bands in the NIR region, which may occur in case of other reflectance materials such as $BaSO_4$ [9].

Catalyst activation and isomerization reactions were carried out in the reaction chamber of the diffuse reflectance attachment and about 160–200 mg of 0.5 wt % Mn-SZ catalyst was supported on a stainless steel grid of the reaction chamber. The detailed procedure for the catalyst preparation is explained in Chapter 3. Activation was performed at 773 K; in He, 50 % O_2/He and O_2 flow with the flow rates of 10, 20 and 30 ml/min from top to bottom over catalyst bed at atmospheric pressure. The temperature was increased with the rate of 5 K/min to 773 K and was kept constant for 30 min and then decreased to 323 K (20 K/min). The total period required for activation was 90 min.

Isomerization reactions were conducted at 323 K and 1 kPa *n*-butane with feed flows between 10 to 30 ml/min and the flow of all gases was controlled by mass flow controllers (Bronckhorst *Hi-TECH* series). The setup for *in-situ* UV-vis-near-IR spectroscopic experiments showing mass flow controllers, spectrometer with the HVC-DR3 reaction chamber and gas chromatography unit is shown in Fig. 2.4

Analysis of the gas phase products of the isomerization reaction was performed by on-line gas chromatography (Varian 3800) using flame ionization detection (FID). Helium was used as a carrier gas and the column used was a PoraPLOT Q column (Chrompack).
The column temperature was increased in steps as the separation proceeds and the time taken for the complete run was ~15 min. The selected temperature program is as follows:

Temp (K)	Rate (K/min)	Hold (min)	Total Time (min)
373	0.0	5.0	5.0
478	20.0	5.0	15.25

For GC calibration two standard gas mixtures containing C_1-C_6 and iso-C_4 at 100 and 1000 vpm concentration (N17 and N18, respectively,) of individual components were used. A PoraPLOT Q column allowed the separation of all alkanes and *iso* – butane in one run, which is shown in Fig. 2.5.

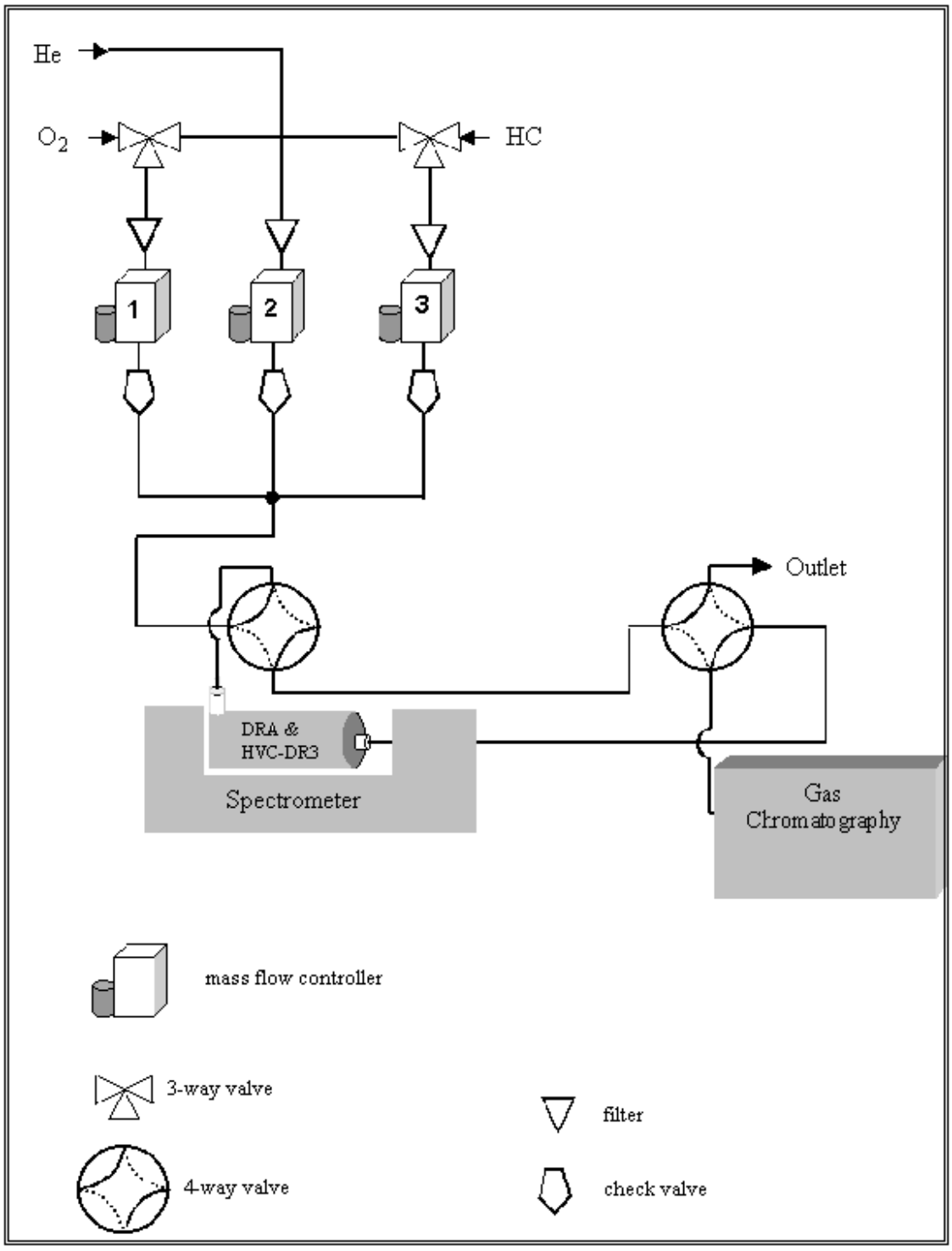

Figure 2.4 Schematic of experimental setup for *in-situ* UV-vis-near-IR diffuse reflectance spectroscopy

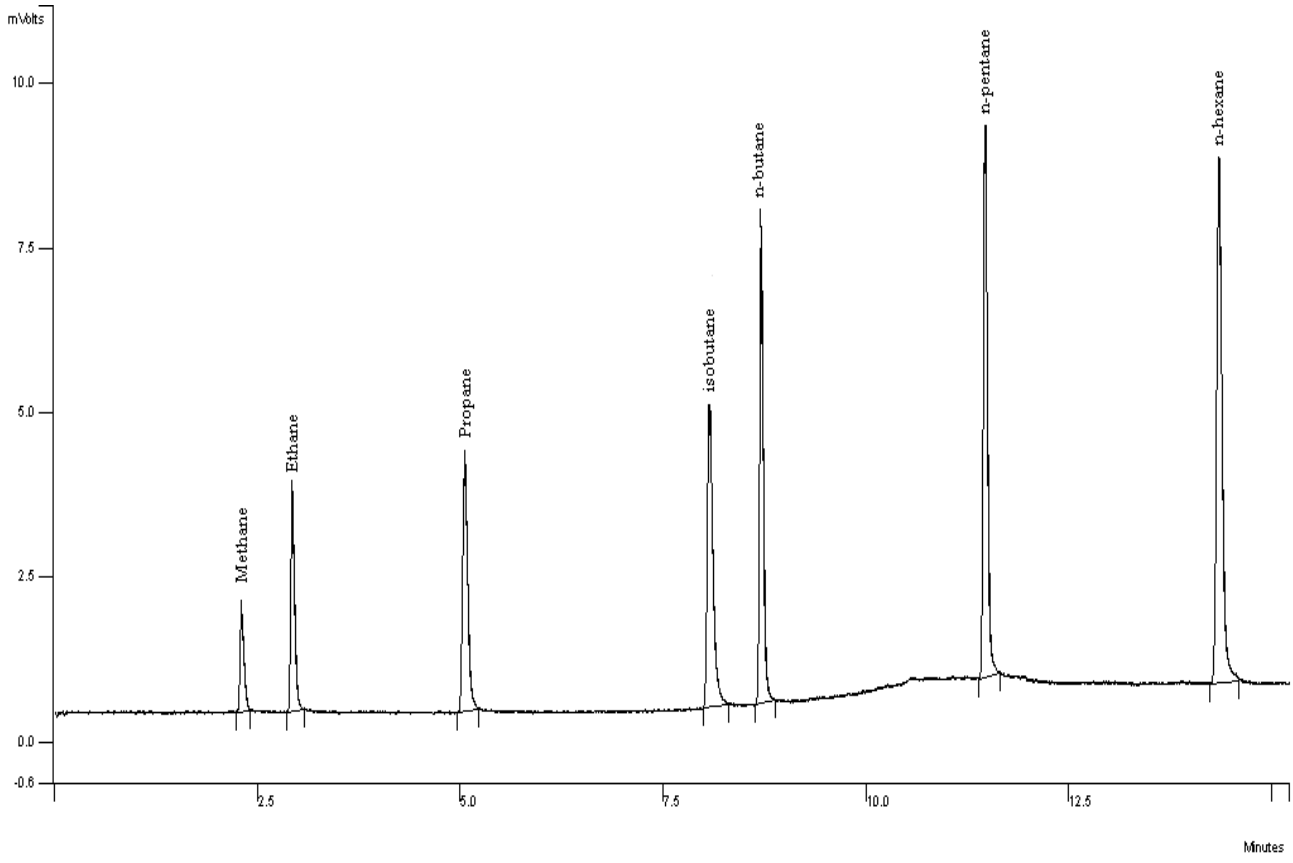

Figure 2.5 Separation of *n*-alkanes from C_1 to C_6 by gas chromatography

2.3.2 Diffuse Reflectance Attachment and Reaction Chamber

The optical configuration of the Harrick Praying Mantis™ Diffuse Reflection Attachment (DRA) is shown in Fig. 2.6. The DRA incorporates two 6:1 90° off-axis ellipsoidal mirrors (M3 and M4), which are arranged with a common focal point, S. Mirrors M1 and M2 transfer the spectrometer beam to the first of these ellipsoids, M3. This ellipsoid focuses the beam on the sample while the ellipsoid M4 collects the diffusely reflected radiation from the sample. This radiation is then directed by mirrors M5 and M6 towards the detector.

Both ellipsoidal mirrors are tilted forward so the diffusely reflected radiation is collected at an azimuthal angle of 120°. This deflects the specularly reflected component behind the collection ellipsoid, minimizing the intensity of restrahlen bands caused by the specularly reflected light. This optical geometry permits collection of up to 20% of all the diffusely reflected radiation, making the DRA quite practical for routine measurements [10].

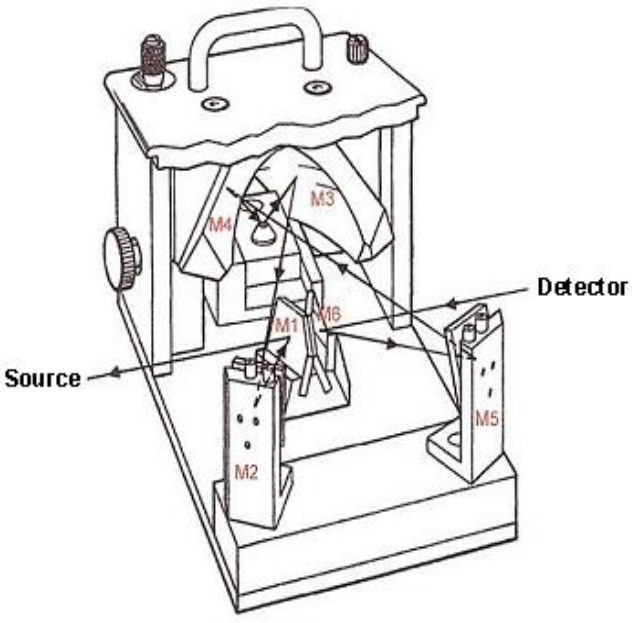

Figure 2.6 Optical configuration of the DRA

In conjunction with the Praying Mantis DRA, a stainless steel high temperature reaction chamber (HVC-DR3) is used which can be heated up to 873 K. It features a middle block with sample cup, a removable dome and three inlet/outlet ports for evacuating the cell and introducing gases (Fig. 2.7). The removable dome has three windows and houses a quartz block.

The chamber can be used under static or dynamic conditions. In the later case, the gas passes through the sample. The temperature of the chamber is controlled with an automatic temperature controller (Harrick). The middle block incorporates a cartridge heater and a K-type thermocouple to achieve the desired temperature of the sample bed. The electrical leads to the heater and thermocouple are located on the outside of the chamber for convenience. A water-cooling jacket is provided to control the temperature of the outer chamber and dome windows during high or low temperature operation.

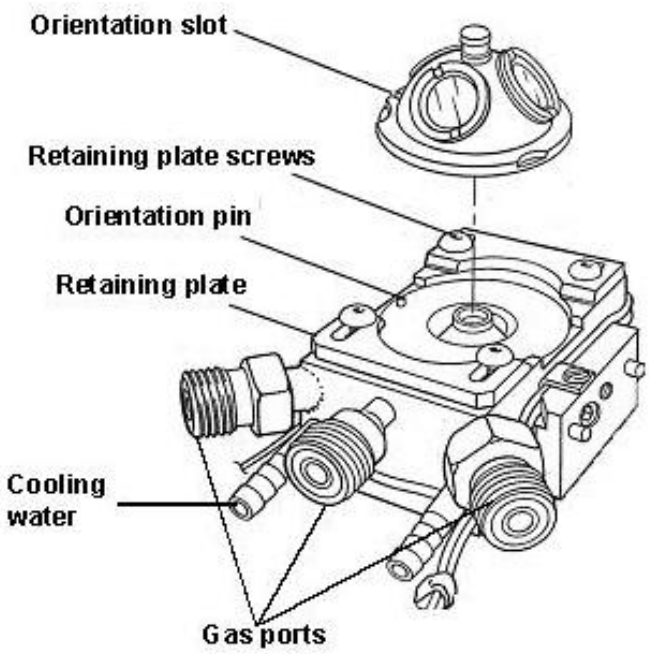

Figure 2.7 Installation of 'dome' in the HVC-DR3 reaction chamber

References

1. B. M. Weckhuysen, Phys. Chem. Chem. Phys., 5 (2003) 4351.
2. M. Scheithauer, E. Bosch, U. A. Schubert, H. Knözinger, T.-K. Cheung, F. C. Jentoft, B. C. Gates and B.Teschez, J. Catal., 177 (1998) 137.
3. A. Bensalem, B. M. Weckhuysen and R. A. Schoonheydt, J. Phys. Chem. B, 101 (1997) 2824.
4. R. Ahmad, J. Melsheimer, F. C. Jentoft and R. Schlögl, J. Catal., 218 (2003) 365.
5. G. Ertl, H. Knözinger, J. Weitkamp, Handbook of Heterogeneous catalysis, ***Vol.2***, Wiley-VCH, 1997.
6. J. D. Lee, Concise Inorganic Chemistry, 4th edition, Chapman & Hall publications, 1991.
7. http://www.piketech.com
8. W. W. Wendlandt, Modern Aspects of Reflectance Spectroscopy, Plenum press, 1968.
9. http://www.labsphere.com
10. http://www.harrricksci.com

Chapter 3

Catalyst Preparation and Characterization

3.1 Preparation of catalyst

3.1.1 Method of preparation

In addition to the fundamental properties that come from the definition of a catalyst i.e. activity and selectivity, industrial applications require that a catalyst be regenerable, reproducible, mechanically and thermally stable and possess suitable morphological characteristics. All these properties significantly depend upon the preparation method of a catalyst. Catalyst preparation is a complex procedure and involves careful control of several unit operations such as precipitation, filtration, washing, forming, drying, impregnation, calcination and activation [5].

For the preparation of Mn-SZ catalyst, mainly two methods have been discussed in the literature namely co-precipitation and impregnation. The co-precipitation method consists of hydrolyzing an aqueous solution containing $ZrO(NO_3)_2$ and $Mn(NO_3)_2$ with NH_4OH, followed by washing drying and sulfation. Impregnated catalysts are prepared by impregnating a metal salt $Mn(NO_3)_2$ on a sulfated zirconium hydroxide support. The metal loading in the finished catalyst is typically 1-5 wt% [2]. Compared to precipitation, impregnation offers a number of advantages:

- The filtering and the wash of the catalyst are eliminated.
- Small metal loadings are easily prepared.
- Impregnation offers some control over the distribution of the metal in pellets.

In the present work, we used the ***incipient wetness method*** (dry impregnation) to prepare Mn-SZ catalyst. In this method, when a liquid (aqueous solution of promoter compound) is slowly added to a porous solid powder (zirconia precursor), the liquid is first absorbed in the pores and the powder will flow as if it is dry. When the pores have been filled the outside of the grains rather suddenly becomes wet, the grains will tend to stick together and the powder will form lumps instead of flowing freely.
The situation when the pores have been filled but the outside of the grains is dry is called incipient wetness and can easily be detected by shaking or stirring the powder [3,4].

3.1.2 Calcination and Activation

In the field of catalysis, calcination is defined as a heat treatment of the catalyst precursor in an oxidizing atmosphere for a couple of hours. The temperature is placed at a level to fully convert the precursor into oxides i.e., to remove all anions except oxygen, and all physical or chemically bound solvent molecules (mostly water). Calcination thus transfers the primary structure, generated by precipitation or impregnation into a composition of higher thermodynamic stability [3].

The importance of the calcination step in the preparation of SZ catalysts is highlighted in many studies. According to Song and Sayari [2], calcination favors the migration of sulfates (SO_4^{2-}) from the bulk to the surface, thus increasing surface acidity. The sulfur content of a SZ catalyst strongly depends on its calcination temperature. Increasing calcination temperature usually results in the gradual removal of sulfur from the catalyst surface, thus decreasing the sulfur content. Thus calcination at an appropriate temperature is crucial to generate the strong acidity in SZ catalysts. The most common calcination temperature ranges from 823 to 923 K.

Calcination may be carried out *in-situ* or *ex-situ*. *In-situ* calcination prevents the catalyst from exposure to ambient atmosphere and keeps the catalyst surface intact, but requires reactors that can withstand high calcination temperatures. On the other hand catalysts may be calcined in a furnace (ex-situ calcination) in static or flowing air, cooled and stored. In this case, it is necessary to pretreat the catalysts such as SZ in the reaction chamber in the range 823-923 K before the reaction.

Activation is defined by IUPAC as the transformation of the precursor solid to the active phase. This is the last but crucial step in catalyst preparation and significantly affects the properties of a particular catalyst such as activity, selectivity and resistance to aging. This is a thermal treatment carried out, before catalytic tests, at very high temperatures (generally in the range 500-723 K). It can be carried out indifferently in a dry air stream, in inert gas or in vacuum either in situ or ex-situ. The purpose of this step is to clean up the surface and bring it to the desired degree of dehydration [1, 2].

3.1.3 Preparation of Sample (0.5 wt% Mn-SZ catalyst)

For the preparation of Mn-SZ catalyst, sulfated zirconium hydroxide with 5-6 % SO_3 (from MEL Chemicals XZO 682/1) was used as a starting material (precursor). The precursor was dried at 383 K for 21 h and cooled in a desiccator. The amount of promoter added corresponded to a concentration of 0.5 wt% metal in the final catalyst. The nitrate solution was added dropwise to the dried precursor under vigorous stirring and the material was dried at room temperature (Sample ID: 654). For calcination, 25 g of this dried sample was filled into a quartz boat and the boat was placed in a 29 mm i.d. quartz tube. The quartz tube was then placed in a tubular furnace (Heraeus RO 4/25) and purged with 200 ml min^{-1} synthetic air. The heating rate was 3 K min^{-1} and the catalyst was treated 3 h at 923 K (Sample ID: 673). Temperature program for calcination is shown in the Fig. 3.1.

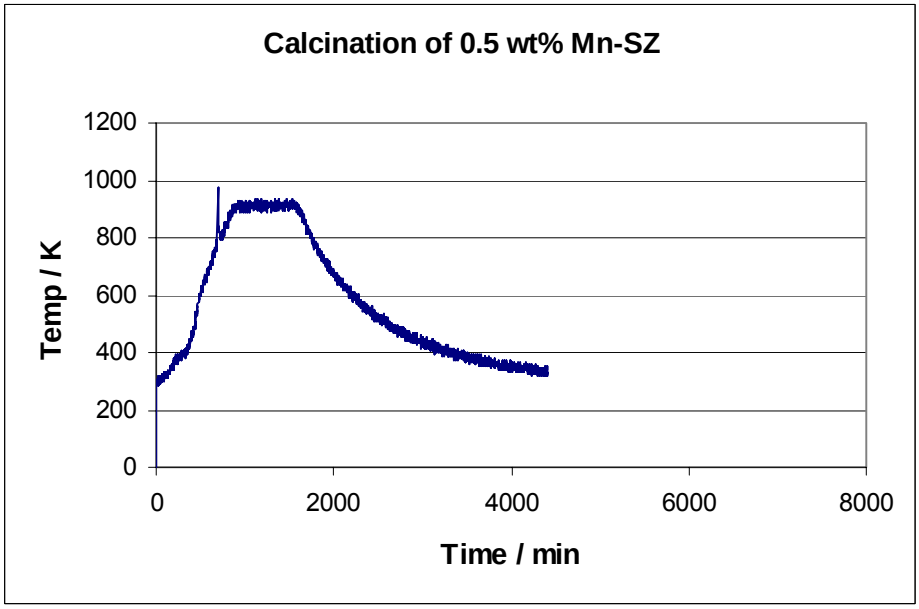

Figure 3.1 Temperature program for calcination

3.2 Catalyst Characterization

Characterization is an important field in catalysis. Spectroscopy, microscopy, diffraction and methods based on adsorption and desorption all offer tools to investigate the nature of an active catalyst. With the knowledge obtained by these methods, one can understand catalysts better and can improve them or even design new catalysts [8]. In the following sections, the characterization techniques utilized in this thesis are presented along with results and discussion.

3.2.1 X-ray Diffraction (XRD)

A) Introduction and Principle

XRD is the most frequently applied technique in catalyst characterization. It is used to identify the various phases in a catalyst and to estimate particle sizes. X-rays are short wavelength electromagnetic radiation produced by deceleration of high energy electrons and/or by electronic transitions in the inner orbitals of atoms. For diffraction applications, only short wavelength X-rays (hard X-rays) in the range of a few angstroms to 0.1 angstrom (1 keV - 120 keV) are used. Because the wavelength of X-rays is comparable to the size of atoms, they are ideally suited for probing the structural arrangement of atoms and molecules in a wide range of materials. The energetic X-rays can penetrate deep into the materials and provide information about the bulk structure.

X-ray diffraction is the elastic scattering of X-ray photons by atoms in a periodic lattice. The scattered monochromatic X-rays that are in phase give constructive interference. This condition is the fulfillment of Braggs law, which is stated as:

$$n\lambda = 2d \sin\theta$$

where, n is the order of reflection (usually assumed 1), λ is the wavelength of Cu-K_α radiation, d is the lattice spacing; θ is the Bragg's angle at which diffraction occurs. Using XRD data, Bragg's law is used to determine the inter-planar spacing from the diffraction peak angular location.

B) Experimental and Results

X-ray diffractograms were recorded in theta-theta geometry on a STOE STADI-P X-ray diffractometer equipped with a focusing primary Ge (111) monochromator and a position sensitive detector, using Cu-K_α radiation (λ = 1.542 Å). For 0.5 wt% Mn-SZ samples the range of 2θ = 20 to 70° was used in order to gain the information about the bulk crystalline phase.

Fig. 3.2 shows a XRD pattern of 0.5 wt% Mn-SZ catalyst calcined at 923 K. It shows the predominant presence of the tetragonal phase of zirconia. Zirconia exhibits three different crystalline polymorphs: monoclinic (*m*), stable at temperatures below 1373 K; tetragonal *(t)* stable at temperatures between 1373 and 2173 K; and cubic (*c*), stable above 2173 K. Nevertheless, the *t* and *c* forms can be generated and maintained as metastable structures at much lower temperatures than those mentioned above [9].

It is reported in the literature that the presence of sulfate during calcination leads to an increased fraction of tetragonal phase in the final product [10]. Also cationic promoters such as Mn are incorporated into the zirconia lattice and stabilize the tetragonal or the cubic phase [11].

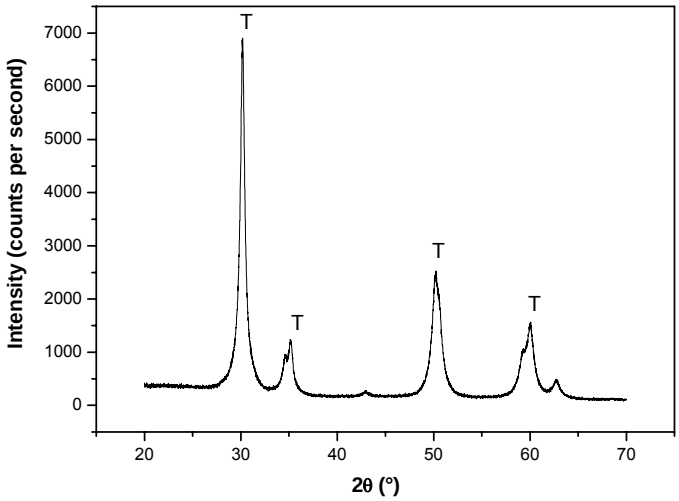

Figure 3.2 XRD pattern of 0.5 wt% Mn-SZ catalyst

3.2.2 Physisorption Analysis

A) Introduction

Porosity and surface area are important characteristics of solid materials that strongly influence the properties and performance of catalysts. Measurements of gas adsorption isotherms are widely used for determining these characteristics and the use of nitrogen (at 77K) as the adsorptive gas is recommended if the sample is nonporous, macroporous or mesoporous [7]. The ***Brunauer-Emmett-Teller (BET)*** method is the most commonly used standard procedure to measure surface areas, in spite of its theoretical limitations and involves the use of the BET equation:

$$\frac{1}{W[(P_0/P) - 1]} = \frac{1}{W_m C} + \frac{(C-1)}{W_m C}\frac{P}{P_0}$$

Where, W is the weight of nitrogen adsorbed at a given P/P_o, and W_m the weight of gas to give monolayer coverage and C, a constant that is related to the heat of adsorption. A linear relationship between $1/W[(P_o/P)-1]$ and P/P_o (BET plot) is required to obtain the quantity of nitrogen adsorbed. This linear portion of the curve is restricted to a limited portion of the isotherm, generally between P/P_o = 0.05-0.30. The slope and intercept are used to determine the quantity of nitrogen adsorbed in the monolayer and used to calculate the surface area. For a single point method, the intercept is taken as zero or a small positive value, and the slope from the BET plot used to calculate the surface area. [7,12].

The instruments that are used to find out the surface area and porosity are called '***Surface Area and Pore Size Analyzers'***. To determine the surface area, they measure solid samples that have been pretreated by some combination of heat, vacuum and/or flowing gas to remove previously adsorbed contaminants. The solid is then cooled, under vacuum conditions, usually to cryogenic temperature. An adsorptive (typically nitrogen) is admitted to the solid in controlled increments. After each dose of adsorptive, the pressure within the surface area analyzer or pore size analyzer is allowed to equilibrate and the quantity of gas adsorbed is calculated.

The gas volume adsorbed at each pressure (at one constant temperature) defines an adsorption isotherm, from which the quantity of gas required to form a monolayer over the external surface of the solid and its pores is determined [13].

B) Experimental and Results

Physisorption measurements were carried out on an 'AUTOSORB -1' surface area analyzer (Quantachrome). Adsorptive properties of the calcined Mn-SZ catalyst have been characterized by N_2 adsorption/desorption at 77 K, results are shown in Fig. 3.3. The isotherm is of Type IV [7, 14], with a steep increment of the adsorbed volume at low pressure and a second one at P/P_0 around 0.5, corresponding to pore filling. The hysteresis loop is representative of an adsorbent with a narrow distribution of relatively uniform mesopores.

The specific surface area of a catalyst calculated from BET plot (Fig. 3.4) is 107.2 m^2/g.

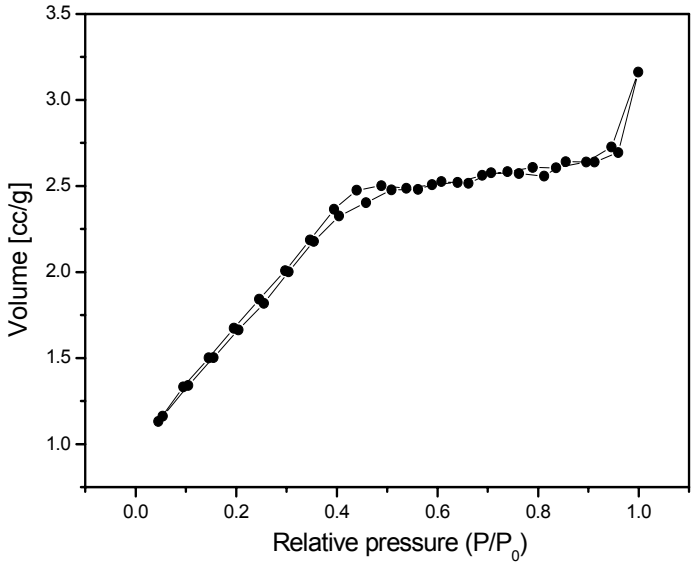

Figure 3.3 N_2 adsorption/desorption isotherm at 77 K

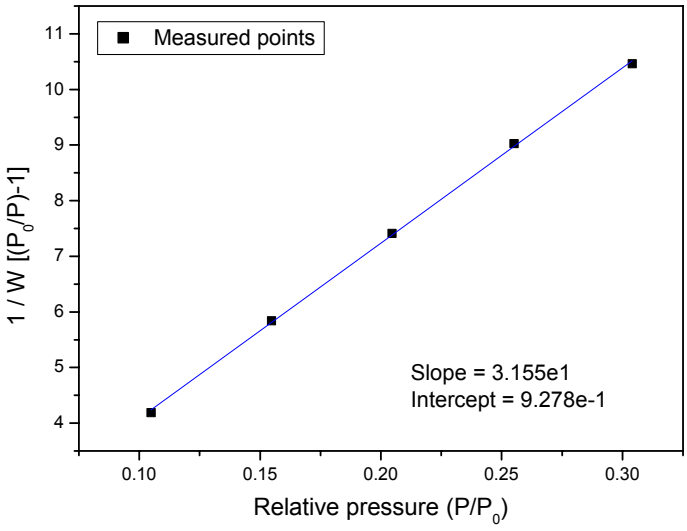

Figure 3.4 BET Plot

3.2.3 Scanning Electron Microscopy (SEM)

A) Introduction

In heterogeneous catalysis, frequently used catalysts are metal particles supported on an oxidic material. The size of the metal particles plays a crucial role for the catalyst efficiency, and the determination of size distribution is one of the main tasks of electron microscopy in catalysis [8]. Field Emission Scanning Electron Microscopy (FE-SEM) is a high-resolution imaging technique providing topographical and structural information in plan view or in cross-section. Often used in conjunction with SEM, Energy Dispersive X-Ray Spectroscopy (EDX) is used to qualitatively and quantitatively analyze the elements present in a selected area of the SEM image. Together FE-SEM and EDX capabilities allow the irradiation by a focused electron beam, imaging secondary or backscattered electrons and energy analysis of x-rays.

Typical SEM applications include plan view and cross-sectional imaging for process development and failure analysis. EDX applications include specific defect analysis or compositional analysis (for boron and heavier elements)

Preparation of the samples is relatively easy since most SEMs only require the sample to be conductive. By scanning an electron probe across a specimen, high resolution images of the morphology or topography of a specimen can be obtained. SEM has a large depth of focus and images at very low or very high magnifications can be obtained [15,16].

B) Experimental and Results

Scanning electron microscopy and energy dispersive X-ray analysis (SEM-EDX) were performed on a Hitachi S-4000 Microscope equipped with a cold field emission gun and energy dispersive X-ray detector system. SEM images and EDX spectra were recorded with acceleration voltages from 3 to 15 kV for Mn-SZ samples.

Fig. 3.5 shows the diagrammatic representation of 0.5 wt% Mn-SZ catalyst bed. After activation in He, the color of the calcined catalyst was changed from light blue to white at the surface of the catalyst bed and white with bluish tinge at the bottom. Figs. 3.6 and 3.7 show SEM images and EDX spectra of the samples taken from the top and bottom of the catalyst bed, respectively, after activation in He.

EDX analysis was carried out to find out the Mn content in the samples taken from the top and bottom of the catalyst bed. But due to very low concentration of Mn (0.5 wt% of the total catalyst), it could not be detected in any of these samples.

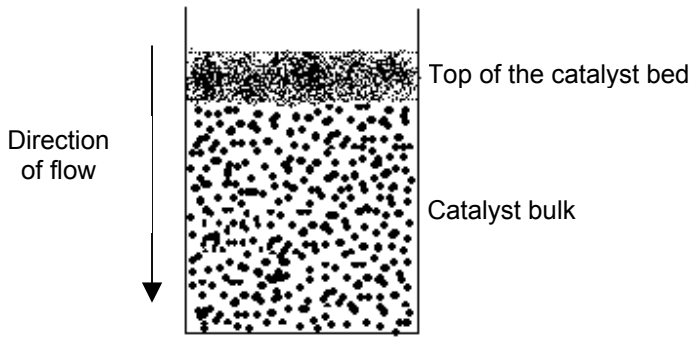

Figure 3.5 Diagram of 0.5 wt% Mn-SZ catalyst bed

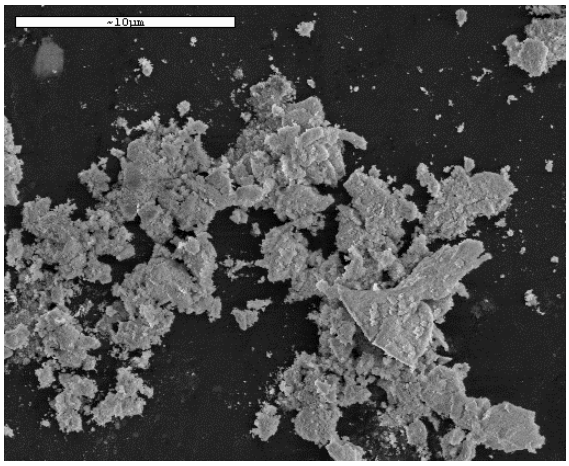

(a) An overview

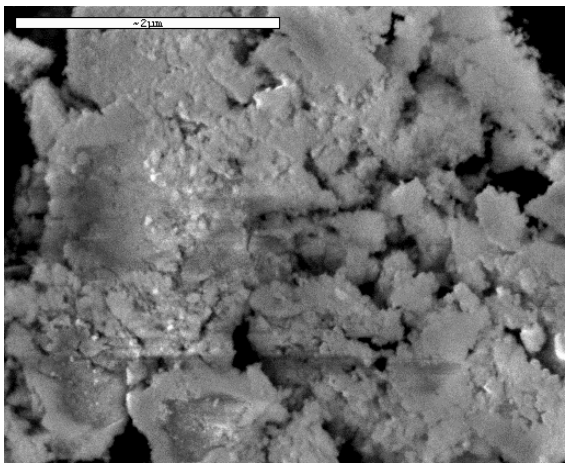

(b) Enlargement of the surface particles

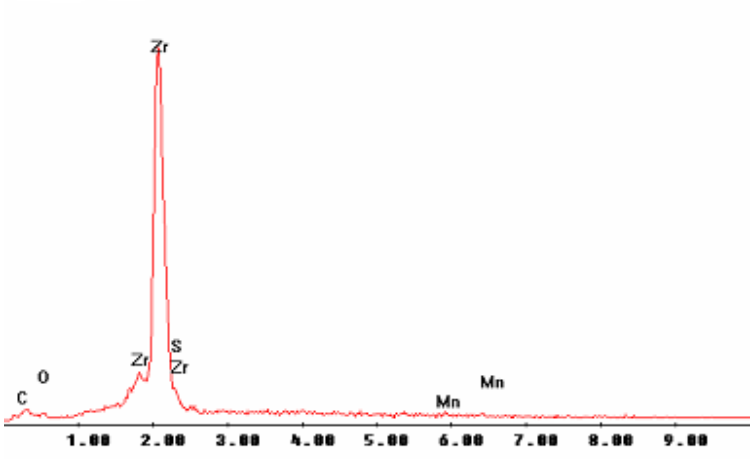

(c) EDX Spectrum

Figure 3.6 SEM pictures and EDX spectrum of the sample taken from the **top** of **the catalyst bed**

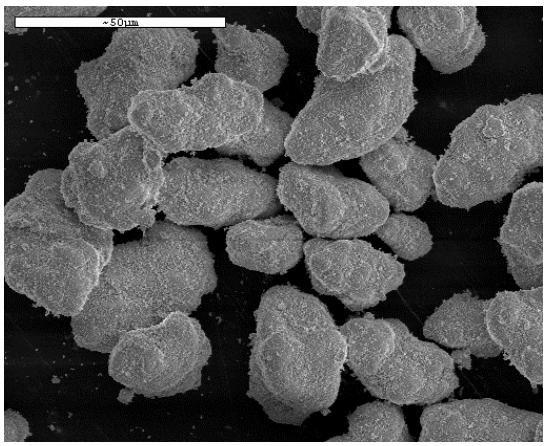

(a) An overview

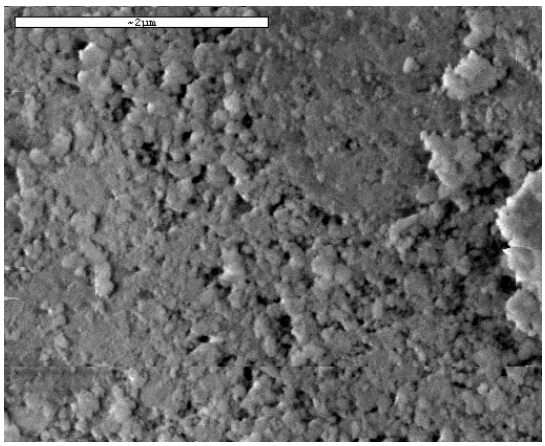

(b) Enlargement of the spherical particles

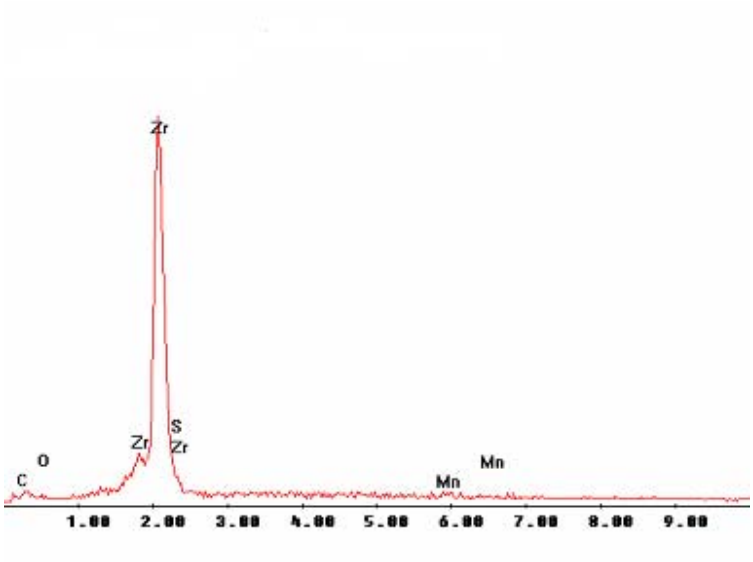

(c) EDX Spectrum

Figure 3.7 SEM pictures and EDX spectrum of the sample taken from the **bottom** of **the catalyst bed**

References

1. G. Ertl, H. Knözinger, J. Weitkamp (Eds.), Preparation of solid catalysts, Wiley-VCH, (1999) 541.
2. X. Song, A. Sayari, Cata. Rev.-Sci. Eng., 38(3) (1996) 329.
3. B. Cornils, W. A. Herrmann, R. Schlögl, Chi-Huey Wong (Eds.), Catalysis from A to Z, A Concise Encyclopedia, Wiley-VCH, (2000) 80.
4. http://www.aue.auc.dk
5. G. Ertl, H. Knözinger, J. Weitkamp (Eds.), Handbook of Heterogeneous catalysis, ***Vol.1***, Wiley-VCH, (1997) 49.
6. G. D. Yadav, J. J. Nair, Microporous and Mesoporous Materials, 33 (1999) 1.
7. G. Ertl, H. Knözinger, J. Weitkamp (Eds.), Handbook of Heterogeneous catalysis, ***Vol.2***, Wiley-VCH, (1997) 427.
8. R. A. van Santen, P. W. N. M. van Leeuwen, J. A. Moulijn, B. A. Averill, Catalysis: An integrated approach, 2nd ed, Elsevier, (1999) 489.
9. R. A. Comelli, C. R. Vera, J. M. Parera, J. Catal., 151 (1995) 96.
10. F. C. Jentoft, A. Hahn, J. Kröhnert, G. Lorenz, R. E. Jentoft, T. Ressler, U. Wild, R. Schlögl, C. Häßner and K. Köhler, J. Catal., 224 (2004) 124.
11. B. S. Klose, R. E. Jentoft, A. Hahn, T. Ressler, J. Kröhnert, S. Wrabetz, X. Yang, and F. C. Jentoft, J. Catal., 217 (2003) 487.
12. http://www.refiningonline.com/EngelhardKB/crep/TCR2_10.htm
13. http://www.globalspec.com
14. X. Yang, F. C. Jentoft, R. E. Jentoft and T. Ressler, Catal. Lett., 81 (2002) 25.
15. http://mse.iastate.edu/microscopy/home.html
16. http://www.accurel.com

Chapter 4

In-Situ UV-vis-NIR Spectroscopic Experiments

4.1 Optimization Experiments

In order to obtain relevant information about the catalyst material, spectroscopic and catalytic measurements have to be done on the *same* catalyst at the *same* time under *optimal* spectroscopic and catalytic conditions [1]. The most important task in the present study was to test a newly installed Harrick Praying Mantis Set-up for *in-situ* UV-vis-NIR investigations of *n*-butane isomerization over Mn-SZ catalyst. In order to fulfill this goal, the following steps had been taken:

- **Blank experiments without catalyst**

- **Optimization of temperature control during reaction**
  - Heating of the dome windows of reaction chamber
- **Optimization of reaction conditions**
  - flow rates, *n*-butane concentration in the feed
- **Test of reproducibility**

4.1.1 Blank experiments without catalyst

n-Butane isomerization reactions were carried out without catalyst at various temperatures and the results obtained are shown in Table 4.1. The temperatures for reaction were increased from 333 K to 523 K, but at none of these temperatures isobutene formed. Thus without catalyst no conversion of *n*-butane to isobutane was observed. Also these results show that, there is no background activity of the *in-situ* cell itself (due to the presence of a thermocouple, metal parts, etc.). No leakage of reagents was observed during reaction.

4.1.2 Optimization of temperature control during reaction

It is not uncommon that the actual temperature at the catalyst bed in the *in-situ* cell is lower or higher than indicated by a temperature read-out. This phenomenon is responsible for lower or higher catalytic performances as would be expected for a real catalytic reactor [1]. These changes in temperatures can also affect the spectroscopic data. To avoid such problems, water cooling jacket surrounding the optical parts of a HVC-DR3 reaction chamber (described in section 2.) was used to heat the outer part of the reaction chamber and the dome windows. These parts were heated to reaction temperature to obtain homogeneous temperature of the catalyst bed and to avoid condensation. Fig. 4.1 shows the effect of heating of dome windows on the rate of isomerization. Curve 2 of fig. 4.1 shows a considerably increased rate of isomerization with the heating of dome windows. A maximum in rate of isomerization was observed very early (after about 4 h time on stream) as compared to the other condition, where the temperature of dome windows was 293 K (room temperature).

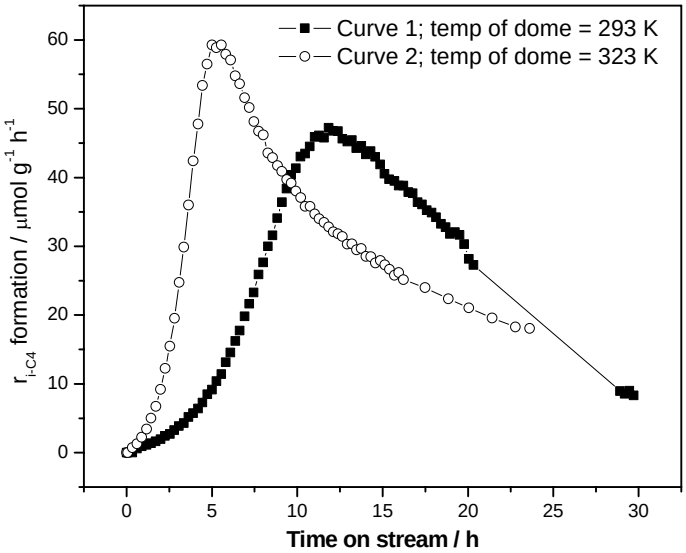

Figure 4.1 Rate of *n*-butane isomerization vs. time on stream. Conditions: 1.77-1.87g Mn-SZ 323 K, Feed: 1 vol% *n*-C_4 in He, 20 ml/min total flow at atmospheric pressure.
Activation in He at 773 K for 30 min.

Table 4.1

Gas chromatography data obtained by *n*-butane isomerization carried out without catalyst at various temperatures. Feed: 1% *n*-C_4 in He (20 ml/min)

Date	Reaction Temp in K	n-butane counts	iso-butane counts
09.07.04	333	322776	-
	-ii-	497980	-
	-ii-	510547	-
	-ii-	508748	-
	-ii-	504603	-
09.07.04	373	386324	-
	-ii-	487835	-
	-ii-	495993	-
	-ii-	493969	-
	-ii-	491909	-
09.07.04	423	482758	-
		493776	-
		494704	-
		494674	-
		495703	-
12.07.04	473	477397	-
		499901	-
		502167	-
		499464	-
12.07.04	523	491810	-
		499703	-
		504744	-
		502386	-

4.1.3 Optimization of reaction conditions

Influence of various flow rates on catalytic performance

The isobutane formation rate plots obtained at 323 K over 0.5 wt % MnSZ catalyst at various **flow rates of feed** (1% *n*-C_4 in He) are shown in Fig. 4.2. Curve 1 of fig. 4.2 shows that, at high flow rate **(30 ml/min)**, the rate of isobutane formation is very high and an induction period of 4 hours is observed. Curve 3 of fig. 4.2 shows that, at low flow rate **(10 ml/min),** the rate of isomerization is very low and an induction period of 12 hours is observed. Hence, for further experiments a medium flow rate **(20 ml/min)** was selected. The rate of isobutane formation was calculated by the following equation:

$$\text{Rate of i-}C_4\text{ formation } [\mu\text{mol g}^{-1}\text{ h}^{-1}] = \frac{\text{ppm}_{\text{i-C4}} \cdot v\ [\text{ml.min}^{-1}] \cdot 6}{2446.5 \cdot m_{cat}\ [\text{g}]}$$

Where, v is total flow rate of the feed and m_{cat} is mass of the catalyst

Influence of feed concentration on catalytic performance

Fig. 4.3 shows the effect of the feed concentration on the rate of isomerization. Curve 1 of figure 4.3 shows that, with higher feed concentration (5% *n*-C_4 in He) the rate of isobutane formation is very high and an induction period of 3 hours is observed. But the catalyst is deactivated very early (after about 5 h time on stream) as compared to the isomerization carried out with lower feed concentration. Thus high activity but faster deactivation is observed with high concentration of feed.

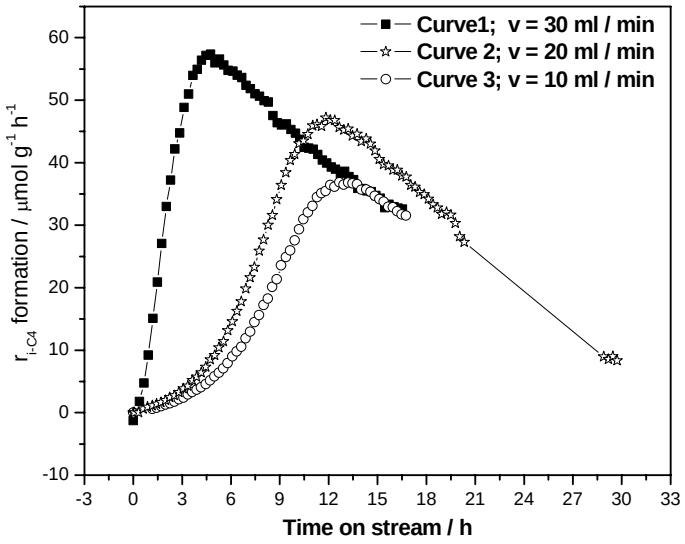

Figure 4.2 Rate of *n*-butane isomerization vs. time on stream. Conditions: 1.48 -1.87 g Mn-SZ (0.5 wt% Mn), 323 K, Feed: 1% *n*-C_4 in He at various flow rates. Activation in He at 773 K for 30 min

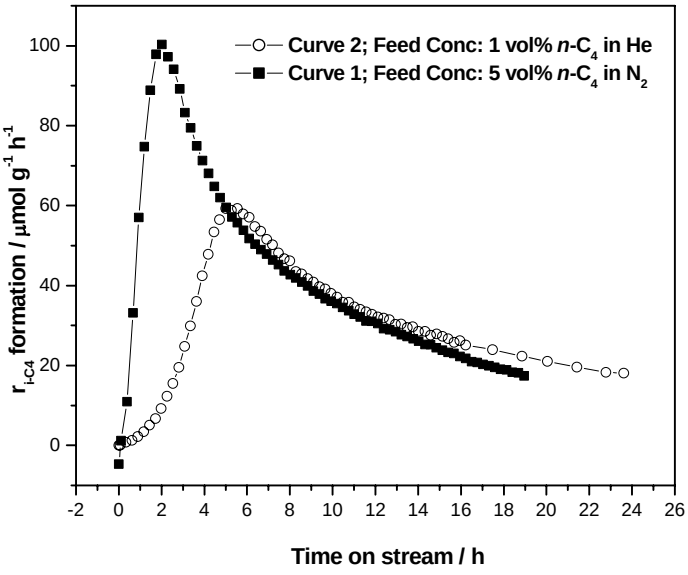

Figure 4.3 Rate of *n*-butane isomerization vs. time on stream. Conditions: 1.77-1.91 g Mn-SZ (0.5 wt% Mn), 323 K, at various feed concentrations, 20 ml/min total flow at atmospheric pressure. Activation in He at 773 K for 30 min.

4.1.4 Test of reproducibility

Fig. 4.4 shows the isomerization rate vs. time-on-stream plots measured at identical reaction conditions (T = 323 K, feed: 1% *n*-C_4 in He) over a 0.5 wt % MnSZ catalyst activated in He. From both experiments (carried out on different days), similar types of reaction profiles were obtained. It is not clear why a remarkable difference in the rate of isomerization was obtained. The graphs show the following characteristics of the reaction profile: An induction period during which the activity slowly increases is observed. The activity then reaches a maximum followed by catalyst deactivation. The deactivation is only partial with a long term activity remaining. During the period of maximum activity, propane and pentanes were observed as by-products in the *n*-butane isomerization, which is consistent with the work reported earlier in our group [2].

Fig. 4.5 shows UV-vis spectra measured after activation of Mn-SZ catalyst in He at 323 K. Blue Curve of figure 4.5 shows a very broad absorption over the entire UV–vis range evolves with two weakly pronounced maxima at 420 and 485 nm. The assignment of these bands is explained in section 4.2. Though we could not reproduce these results we observed similar trend for the activation experiments carried out in inert atmosphere.

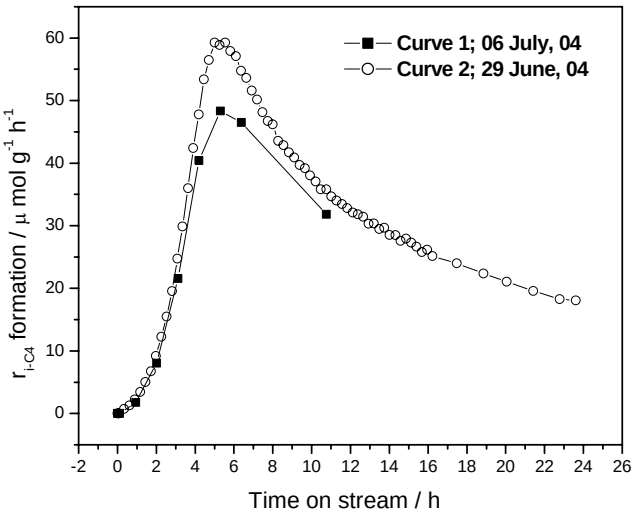

Figure 4.4 Rate of *n*-butane isomerization vs. time on stream. Conditions: 1.72 -1.77 g Mn-SZ, 323 K, Feed: 1% *n*-C_4 in He (20 ml/min), Activation in He at 773 K for 30 min.

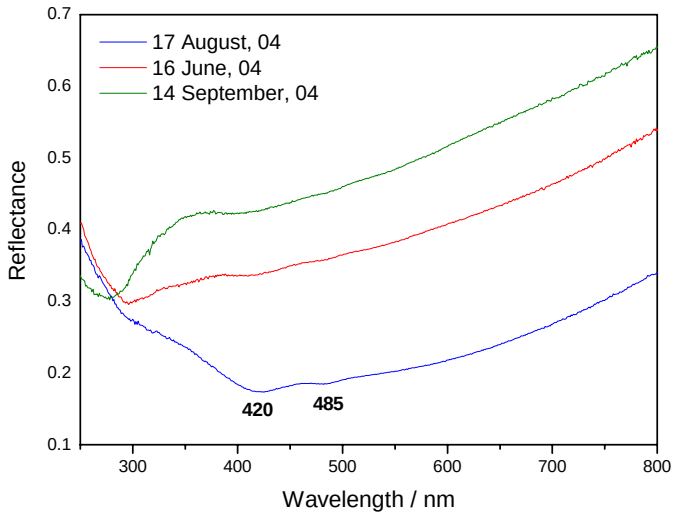

Figure 4.5 UV–vis spectra of Mn-SZ after activation in He (20 ml/min) at 323 K.

4.2 Activation of Mn-SZ catalyst

The experimental details of the activation of Mn-SZ catalyst are explained in Chapter 2 (Section 2.3.1). Fig. 4.6 shows UV-vis-NIR spectra of the catalyst before and after activation in He. The NIR region of the spectrum shows two prominent bands at 1425 and 1920 nm of adsorbed water. These bands are not seen after activation (red curve of Fig.4.6) and the catalyst is largely dehydrated.

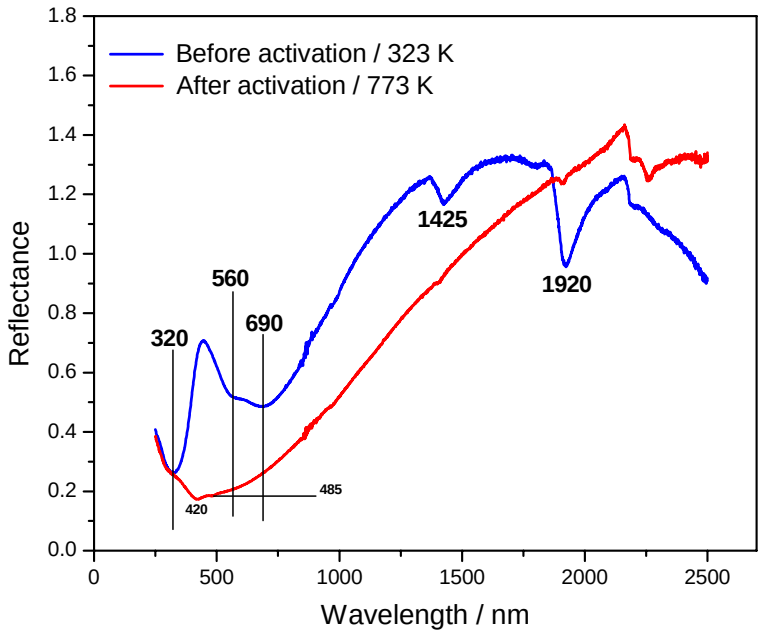

Figure 4.6 UV-vis-NIR spectra of Mn-SZ before and after activation in He

UV-vis spectra of the calcined Mn-SZ catalyst during activation in He are shown in Fig. 4.7. The spectrum taken at 341 K shows one strong absorption located at 320 nm and at least two overlapping bands with maxima at about 560 and 690 nm.

The band at 320 nm can be assigned to a charge transfer from O^{2-} to Mn^{3+} [3], the band around 560 nm to a d-d transition of Mn^{2+} or Mn^{3+} [4] and the band at the highest wavelength to a d-d transition of Mn^{3+} [5]. Mn^{2+} d-d transitions are spin-forbidden [4] and should be weak; however, such transitions should contribute to the spectra because the average Mn valence in these catalysts according to XAFS is around 2.65 [6]. The intensity of the d-d bands decreases with increasing temperature and broadening lets them appear to be one band.

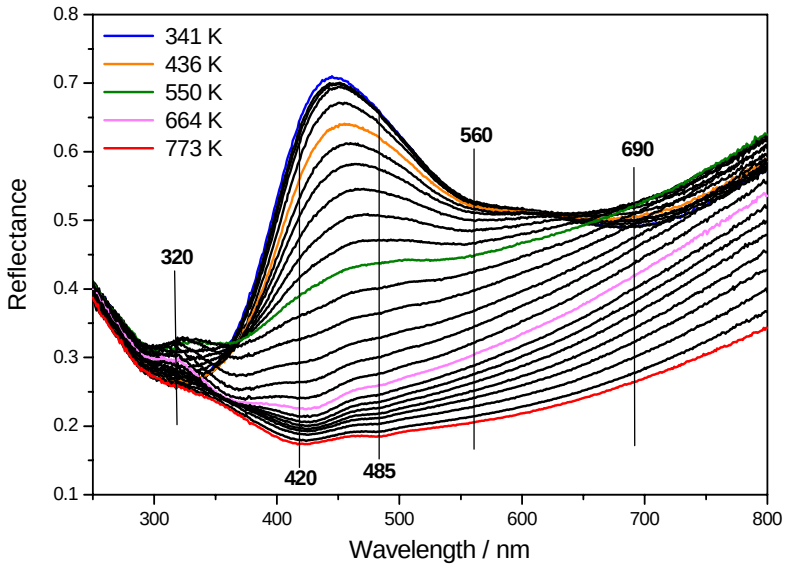

Figure 4.7 UV–vis spectra of Mn-SZ during activation in He

A very broad absorption over the entire UV–vis range evolves with two weakly pronounced maxima at 420 and 485 nm. The band at 420 nm is characteristic of Mn^{2+} in octahedral environment [7], the band at 485 nm has been reported for Mn^{2+} [7] and for Mn^{3+} [3], which was also seen in the analysis of the reference compounds (MnO, Mn_2O_3), Fig. 4.8.

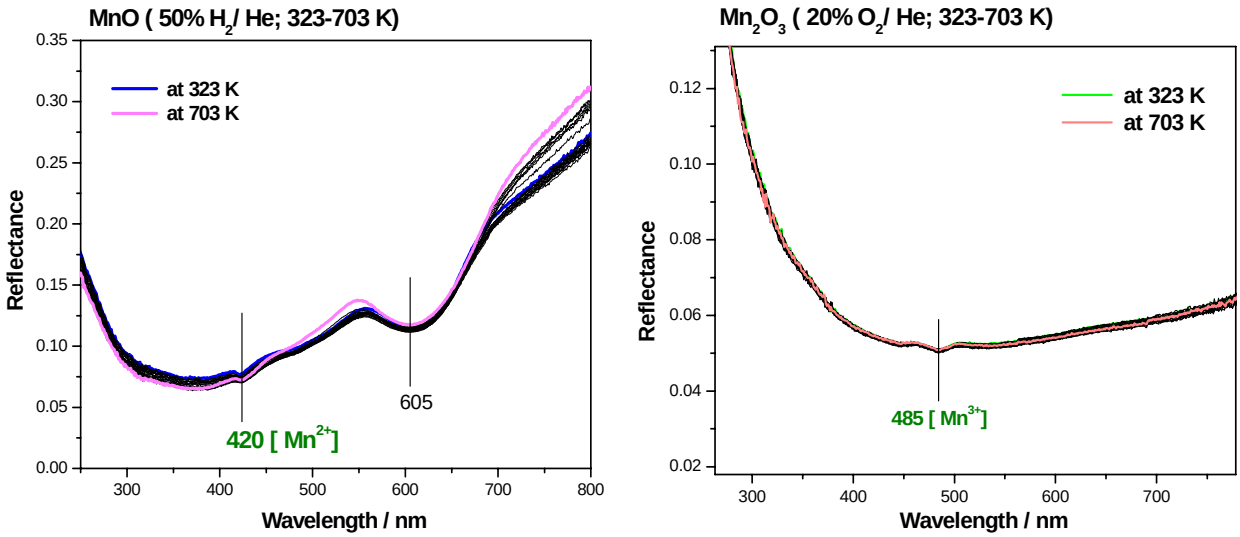

Figure 4.8 Analysis of Reference Compounds

Activation in O_2 and in 50% O_2/He also dehydrates the catalyst as in He. This can be clearly seen in the NIR region of the spectra before and after activation (Figs. 4.9 (a) and 4.10 (a)). In UV-vis spectra (Figs. 4.9 (b) and 4.10 (b)), broadening of d-d transition bands at 560 and 690 nm is observed, however no new bands appear.

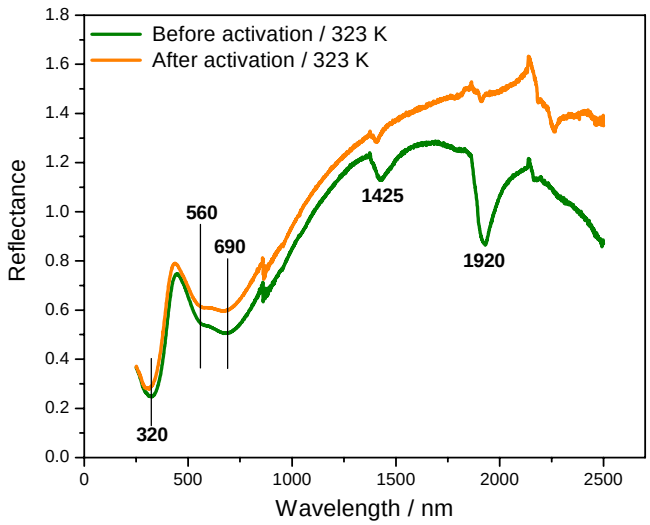

Figure 4.9(a) UV–vis-NIR spectra of Mn-SZ before and after activation in O_2

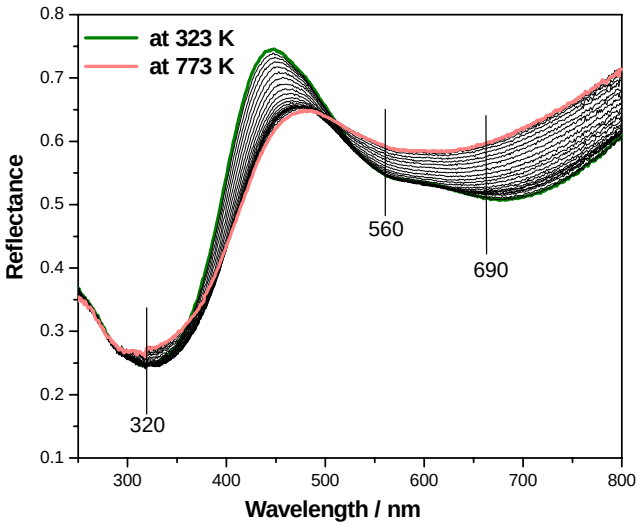

Figure 4.9(b) UV–vis spectra of Mn-SZ during activation in O_2

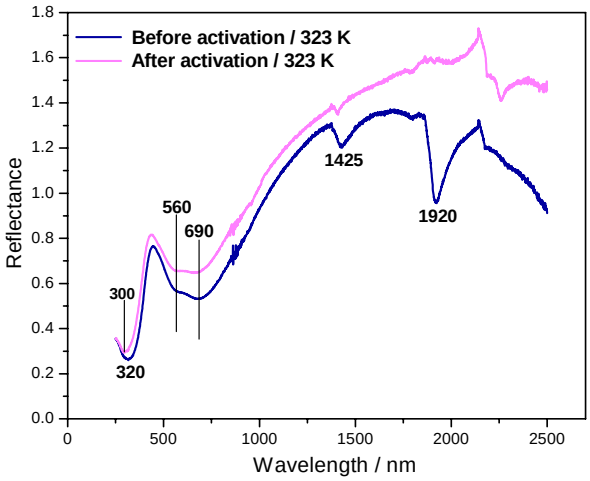

Figure 4.10(a) UV–vis-NIR spectra of Mn-SZ before and after activation in 50% O_2/He

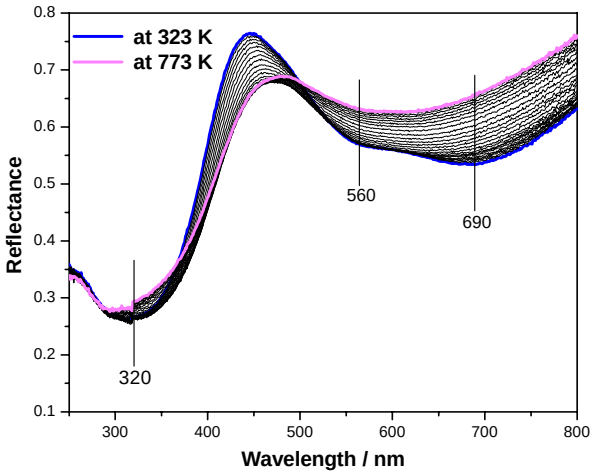

Figure 4.10(b) UV–vis spectra of Mn-SZ during activation in 50% O_2/He

Comparison of the spectra obtained after activation in inert (He) and oxidizing atmosphere is shown in Fig. 4.11. In its initial state, i.e. after calcination and exposure to ambient conditions, the catalyst contains mainly Mn^{3+} and presumably small amount of Mn^{2+} as well as adsorbed water. Activation in O_2 only dehydrates the catalyst, while activation in He additionally leads to partial reduction of manganese (formation of new species Mn^{2+}). Thus the main process during activation in oxygen containing atmosphere is dehydration.

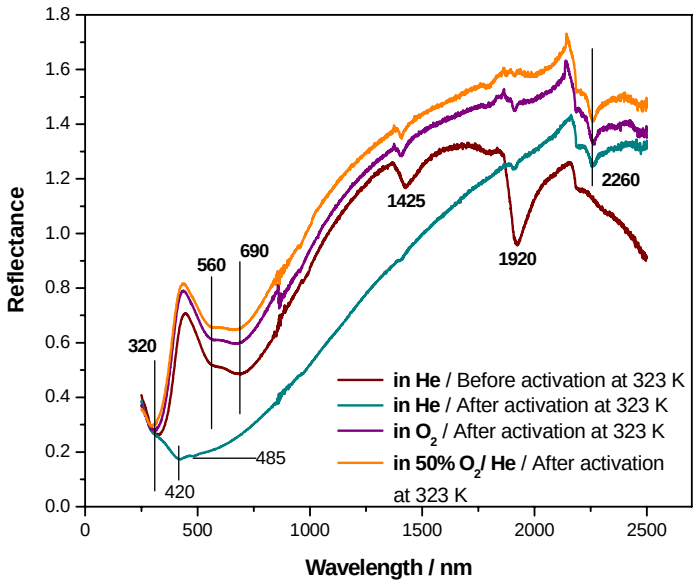

Figure 4.11 Activation of Mn-SZ in He and in O_2

4.3 Influence of activation conditions on catalytic performance

Wan [9] and Song and Kydd [10] reported that Fe-Mn-promoted SZ catalysts are more active after activation in oxidizing conditions, which was seen as evidence for an oxidative dehydrogenation (ODH) initiation reaction. Our results were also found to be in agreement with their findings. Mn-SZ (0.5 wt% Mn) catalyst activated in 100% O_2 exhibits a maximum isomerization rate of 220 µmol $g^{-1}h^{-1}$ (Fig. 4.13); activation in inert gas only yields a maximum rate of 100 µmol $g^{-1}h^{-1}$(Fig. 4.12). With time on stream, the catalysts first passes through a phase of rapidly increasing conversion (induction period), then through a conversion maximum followed by partial deactivation to a steady state.

The length of induction period is strongly dependent on reaction conditions such as *n*-butane concentration in the feed, and the reaction temperature. The activity decrease following the induction period is due to increased surface concentration of olefins leading to coke formation [8]. However, *in-situ* UV–vis-NIR spectra measured during *n*-butane isomerization (Figs. 4.14 and 4.15) show no evidence for coke formation or unsaturated species on the surface of Mn-SZ catalyst. Ahmad et al. [2] investigated sulfated zirconia that had been deactivated during *n*-butane isomerization and found a band at 310 nm. This band ascribed to unsaturated species was not observed in our results.

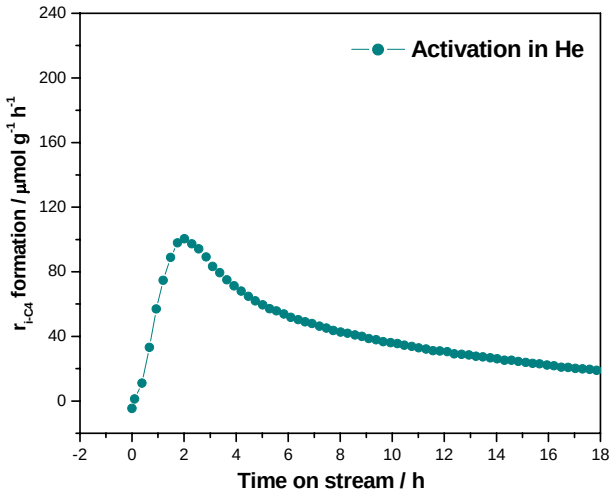

Figure 4.12 Rate of *n*-butane isomerization vs. time on stream. Conditions: 1.91 g Mn-SZ, 323 K, Feed: 5% *n* -C_4 in N_2 (20 ml/min), **Activation in He** at 773 K for 30 min.

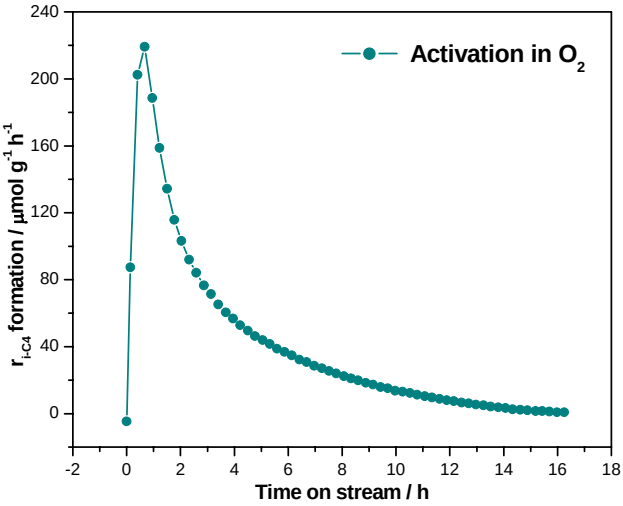

Figure 4.13 Rate of *n*-butane isomerization vs. time on stream. Conditions: 1.99 g Mn-SZ, 323 K, Feed: 5% *n* -C_4 in N_2 (20 ml/min), **Activation in O_2** at 773 K for 30 min.

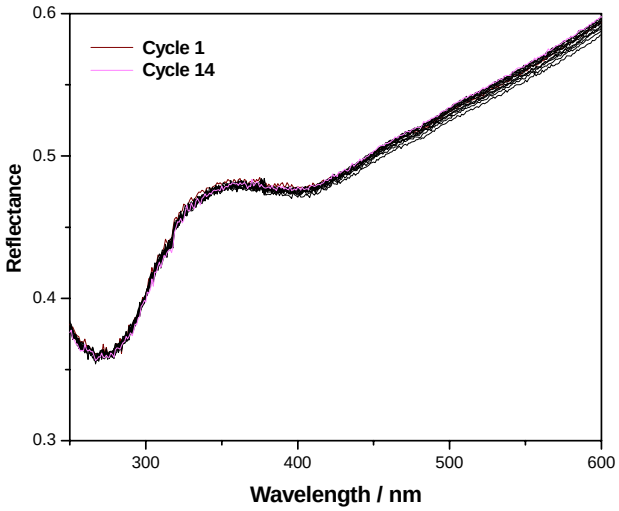

Figure 4.14 UV-vis spectra of Mn-SZ recorded *in-situ* during *n*-butane isomerization. Conditions: 1.91 g Mn-SZ, 323 K, Feed: 5% *n* -C_4 in N_2 (20 ml/min), **Activation in He** at 773 K for 30 min.

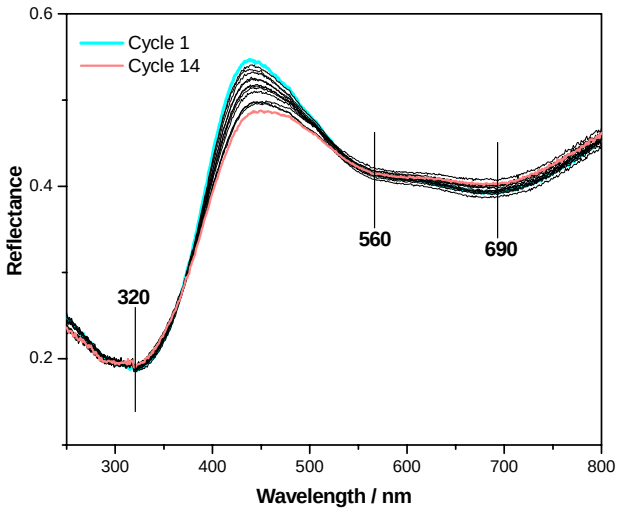

Figure 4.15 UV-vis spectra of Mn-SZ recorded during *n*-butane isomerization. Conditions: 1.99 g Mn-SZ, 323 K, Feed: 5% *n* -C_4 in N_2 (20 ml/min), **Activation in O_2** at 773 K for 30 min.

References

1. B. M. Weckhuysen, *In-Situ* Spectroscopy of Catalysts, American Scientific Publications, 1st ed. (2004) 6.
2. R. Ahmad, J. Melsheimer, F. C. Jentoft and R. Schlögl, J. Catal., 218 (2003) 365.
3. F. Milella, J.M. Gallardo-Amores, M. Baldi, G. Busca, J. Mater. Chem., 8(11), (1998) 2525.
4. W. Sjoerd Kijlstra, E.K. Poels, A. Bliek, B.M. Weckhuysen, R.A. Schoonheydt, J.Phys. Chem. B, 101 (1997) 309.
5. E. Fernández López, V. Sánchez Escribano, C. Resini, J.M. Gallardo-Amores, G. Busca, Appl. Catal. B: Environmental, 29 (2001) 251.
6. R.E. Jentoft, A.H.P. Hahn, F.C. Jentoft, T. Ressler, submitted to Phys. Chem. Chem. Phys.
7. G.W. Pratt, Jr., Phys. Rev., 2 (1959) 281.
8. X. Song, A. Sayari, Cata. Rev.-Sci. Eng., 38(3) (1996) 329.
9. K.T. Wan, C.B. Khouw, M.E. Davis, J. Catal., 58 (1996) 311.
10. S.X. Song, R.A. Kydd, Catal. Lett., 51 (1998) 95.

Chapter 5

Summary and Outlook

The results of optimization experiments showed that the newly installed Harrick Praying Mantis Set-up is suitable for *in-situ* UV-vis-NIR studies of *n*-butane isomerization over Mn-SZ catalyst. The investigation of Mn-SZ during activation in inert (He) and oxidizing atmosphere (O_2) at 773 K by *in-situ* UV-vis-NIR diffuse reflectance spectroscopy revealed important information on the oxidation state of the manganese. In its initial state, i.e. after calcination and exposure to ambient conditions, the catalyst contains mainly Mn^{3+} and presumably small amounts of Mn^{2+} as well as adsorbed water. Activation in O_2 only dehydrates the catalyst, while activation in He additionally leads to partial reduction of manganese (formation of new species Mn^{2+}). The different sensitivity to the activation conditions suggests that Mn and the surface functionalities (hydroxyls, sulfate) are independent of each other.

Fe-Mn-promoted SZ catalysts are more active after activation in oxidizing conditions, which was seen as evidence for an oxidative dehydrogenation (ODH) initiation for *n*-butane isomerization [1,2]. We also found a similar relationship between catalyst performance and activation. Mn-SZ activated in pure O_2 exhibits a maximum isomerization rate of 220 µmol $g^{-1}h^{-1}$; activation in He only yields a maximum rate of 100 µmol $g^{-1}h^{-1}$. With time on stream, the catalyst first passes through a phase of rapidly increasing conversion (induction period), then through a conversion maximum followed by partial deactivation to a steady state. During the period of maximum activity, propane and pentanes were observed as by-products.

Induction period was found to depend on the activation atmosphere and the *n*-butane concentration in the feed. Song and Sayari [3] reported that the activity decrease following the induction period is due to increased surface concentration of olefins leading to coke formation. In our case, no evidence for formation of coke or unsaturated species on the surface of Mn-SZ catalyst was found by *in-situ* UV–vis-NIR spectra measured during *n*-butane isomerization.

To conclude, *in-situ* UV–vis-NIR diffuse reflectance spectroscopy proved extremely helpful in monitoring the changes of the manganese oxidation state and water content during activation and *n*-butane isomerization. However, the role of Mn is not completely resolved and further experiments will be needed to prove or disprove ODH initiation and to give the causes of catalyst deactivation.

References

1. K.T. Wan, C.B. Khouw, M.E. Davis, J. Catal., 58 (1996) 311.
2. S.X. Song, R.A. Kydd, Catal. Lett., 51 (1998) 95.
3. X. Song, A. Sayari, Cata. Rev.-Sci. Eng., 38(3) (1996) 329.

The work in this thesis has been or will be published in due course.

Papers:

1. F.C. Jentoft, B.S. Klose, R.E. Jentoft, T. Ressler, P. Joshi, A.Trunschke, and R. Schlögl
   Deactivation and Regeneration of Mn-Promoted Sulfated Zirconia Alkane Isomerization Catalysts: An In-Situ Spectroscopic Study.
   In Proceedings of the DGMK International Conference: "C_4/C_5-Hydrocarbons: Routes to higher value-added products", Munich, Germany, Oct 13-15, 2004. ISBN: 3-936418-23-3, 23-30.

2. F. C. Jentoft, P. Joshi, C. Chan Thaw, B. S. Klose, R. E. Jentoft, T. Ressler
   A. Trunschke and R. Schlögl
   In Situ Spectroscopic Analysis of Role of Manganese in Promoted Sulfated Zirconia for Initiation of Butane Isomerization.
   Accepted for oral presentation at XXXVIII. Jahrestreffen Deutscher Katalytiker Weimar, Germany, 16 – 18, March 2005.

3. F. C. Jentoft, B. S. Klose, R. E. Jentoft, T. Ressler, P. Joshi, C. Chan Thaw,
   A.Trunschke and R. Schlögl
   Initiation of Alkane Isomerization on Sulfated Zirconia Catalysts Studied by In Situ X-ray Absorption, UV-vis and IR Spectroscopy.
   Communicated for 19th North American Catalysis Society Meeting to be held in Philadelphia, Pennsylvania, U.S.A., May 22-27, 2005.

Posters:

1. F.C. Jentoft, B.S. Klose, A.Trunschke P. Joshi, and R. Schlögl
   In Situ DRIFT and UV-vis Spectroscopic Investigation of Mn-Promoted Sulfated Zirconia during Alkane Isomerization.
   Third International Taylor Conference on Catalysis at the Interface: Challenges and Opportunities, Belfast, UK, 5-8 September, 2004.